



**HAL**  
open science

## Structural and functional diversity of type IV secretion systems

Tiago R D Costa, Jonasz B Patkowski, Kévin Macé, Peter J. Christie, Gabriel Waksman

► **To cite this version:**

Tiago R D Costa, Jonasz B Patkowski, Kévin Macé, Peter J. Christie, Gabriel Waksman. Structural and functional diversity of type IV secretion systems. *Nature Reviews Microbiology*, 2024, 22 (3), pp.170-185. 10.1038/s41579-023-00974-3 . hal-04284264

**HAL Id: hal-04284264**

**<https://hal.science/hal-04284264>**

Submitted on 18 Dec 2023

**HAL** is a multi-disciplinary open access archive for the deposit and dissemination of scientific research documents, whether they are published or not. The documents may come from teaching and research institutions in France or abroad, or from public or private research centers.

L'archive ouverte pluridisciplinaire **HAL**, est destinée au dépôt et à la diffusion de documents scientifiques de niveau recherche, publiés ou non, émanant des établissements d'enseignement et de recherche français ou étrangers, des laboratoires publics ou privés.



Distributed under a Creative Commons Attribution - NonCommercial 4.0 International License

1  
2  
3  
4  
5  
6  
7  
8  
9  
10  
11  
12  
13  
14  
15  
16  
17  
18

## Structural and functional diversity of type IV secretion systems

Tiago R. D. Costa<sup>1,\*</sup>, Jonasz B. Patkowski<sup>1</sup>, Kévin Macé<sup>2,3</sup>, Peter J. Christie<sup>4,\*</sup> and Gabriel Waksman<sup>2,\*</sup>

<sup>1</sup> Centre for Bacterial Resistance Biology, Department of Life Sciences, Imperial College, London, UK

<sup>2</sup> Institute of Structural and Molecular Biology, Birkbeck and UCL, London, UK

<sup>3</sup> Institut de Génétique et Développement de Rennes (IGDR), Université de Rennes, CNRS, Rennes, France

<sup>4</sup> Department of Microbiology and Molecular Genetics, McGovern Medical School at UTHealth, Houston, Texas,

USA

E-mails:

[t.costa@imperial.ac.uk](mailto:t.costa@imperial.ac.uk);

[peter.j.christie@uth.tmc.edu](mailto:peter.j.christie@uth.tmc.edu);

[g.waksman@ucl.ac.uk](mailto:g.waksman@ucl.ac.uk); [g.waksman@bbk.ac.uk](mailto:g.waksman@bbk.ac.uk)

19 **Abstract**

20 Considerable progress has been made in recent years in the structural and molecular biology of type IV secretion  
21 systems (T4SSs) in Gram-negative bacteria. The latest advances have substantially improved our understanding  
22 of the mechanisms underlying the recruitment and delivery of DNA and protein substrates to the extracellular  
23 environment or target cells. In this Review, we aim to summarize these exciting structural and molecular biology  
24 findings, and to discuss their functional implications for substrate recognition, recruitment and translocation as  
25 well as the biogenesis of extracellular pili. We also describe adaptations necessary for deploying a breadth of  
26 processes, such as bacterial survival, host–pathogen interactions, and biotic and abiotic adhesion. We highlight  
27 the functional and structural diversity of this extremely versatile secretion superfamily to function under  
28 different environmental conditions and in different bacterial species. Additionally, we emphasise the  
29 importance of further understanding the mechanism of type IV secretion, which will support us in combating  
30 antimicrobial resistance and treating T4SS-related infections.

## 31 [H1] Introduction

32 Type IV secretion systems (T4SSs) are a family of highly complex and versatile nanomachines that span the entire  
33 cell envelopes of Gram-positive and Gram-negative bacteria as well as Archaea <sup>1-3</sup> (Figure 1). They function in  
34 two main capacities, as DNA transfer (conjugation) systems or as protein effector translocators<sup>4,5</sup>, generally  
35 mediating transfer of macromolecules by mechanisms requiring direct donor–target cell contact. A few systems  
36 have evolved the capacity to export DNA or protein substrates to the extracellular milieu, or to take up DNA  
37 from it. Many T4SSs also elaborate surface organelles such as conjugative pili or surface adhesins to promote  
38 attachment and biofilm formation, but there are also examples of T4SSs that seem to have lost the capacity to  
39 translocate substrates and instead function only in adhesion. Considering this enormous range of biological  
40 activities, the T4SSs are exceptionally important from a medical perspective. Accordingly, they are increasingly  
41 viewed as viable targets for therapeutic intervention to thwart the spread of conjugation-driven antibiotic  
42 resistance and infection by pathogens <sup>6,7</sup>.

43

44 T4SSs in Gram-negative species are composed minimally of 12 core subunits that are generically termed VirB1 -  
45 VirB11 and VirD4 (Ref. <sup>8</sup>). Systems assembled only with the core VirB–VirD4 components are considered  
46 ‘minimized’, and many of these systems function as conjugation machines by delivering DNA substrates to target  
47 bacteria<sup>9,10</sup>. Over the course of evolution, T4SSs have acquired several additional protein components that are  
48 integrated into the core structure composed of VirB and VirD4 proteins. As a result, assembly of an expanded  
49 T4SS may require up to 25 different proteins <sup>10,11</sup>. Some of these expanded systems can mediate conjugative  
50 DNA transfer, but many have acquired new functionalities relating to translocation of effector proteins or toxins,  
51 with or without retention of the ancestral DNA transfer function<sup>12,13</sup>.

52

53 In recent years, our understanding of the architectures and mechanisms of actions of T4SSs has increased  
54 substantially, most notably by implementation of state-of-the art microscopy techniques including cryo-electron  
55 microscopy (cryo–EM), cryo-electron tomography (cryo–ET) and fluorescence microscopy. These studies have  
56 enabled visualization of major machine subassemblies and conjugative pili at or near atomic resolution or fully  
57 intact T4SSs in the native context of the bacterial cell envelope at lower resolutions (Supplementary Table 1).  
58 Most exciting, a very recent study defined for the first time the architecture of a nearly completely intact  
59 minimised T4SS encoded by the conjugative plasmid R388 (Ref. <sup>14</sup>). There also has been considerable progress  
60 in defining the architecture and mechanisms of action of the VirD4 components of T4SSs; these ATPases have  
61 crucial roles in recruiting and coupling substrates to the translocation channel and hence are termed type IV  
62 coupling proteins (T4CPs). Finally, studies applying a combination of *in situ* cryo-ET and fluorescence microscopy  
63 have advanced our knowledge of T4SS assembly dynamics and spatial organization within intact cells.

64

65 This Review will primarily focus on the T4SSs found in Gram-negative bacteria, as they have been the most  
66 extensively characterized in terms of both structure and function. We will summarise the current knowledge of  
67 paradigmatic T4SSs functioning in these bacteria with a focus on their architectures and adaptations for  
68 specialised functions. We also update the reader on recent studies exploring the biogenesis pathways and spatial

69 localization of T4SSs, and we conclude with a brief review of progress toward developing small molecule  
70 inhibitors of T4SSs and manipulating these versatile nanomachines for novel therapeutic ends.

71

## 72 [H1] Architectures of minimised systems

73 Early biochemical studies supplied evidence that the VirB subunits VirB7, VirB9 and VirB10 assemble as a  
74 stabilizing structural scaffold for the T4SS; this scaffold ultimately was designated as the outer membrane core  
75 complex (OMCC)<sup>8,15</sup>. OMCCs are intrinsically stable and amenable to isolation for structural characterization.  
76 Accordingly, over a decade ago, high-resolution structures were presented for the OMCC associated with a  
77 minimized T4SS elaborated by the conjugative plasmid pKM101 (T4SS<sub>pKM101</sub>)<sup>16,17</sup>, and soon afterwards for several  
78 other OMCCs from minimized systems<sup>18-21</sup>. The most recent structure presented for the nearly intact T4SS  
79 encoded by plasmid R388 (T4SS<sub>R388</sub>) now has provided important refinements of these earlier structures<sup>14</sup>  
80 (Figure 2a). The OMCC from the T4SS<sub>R388</sub> presents as a barrel-shaped structure of 130 Å in height and 185 Å in  
81 width. It is composed of an outer and inner layer that are designated as the O-layer and I-layer, respectively.  
82 Remarkably, in contrast to the lower-resolution structures obtained previously, the new structure shows that  
83 the O- and I-layers have different symmetries (Figure 2a). The O-layer is made up of 14 copies of homologs of  
84 the VirB7 lipoprotein and C-terminal domains (CTDs) of the VirB9- and VirB10-like subunits. VirB7 anchors the  
85 OMCC to the outer membrane via its N-terminal lipid modification. The I-layer assumes a 16-fold symmetry,  
86 formed by copies of N-terminal domains (NTDs) of the VirB9 and VirB10 subunits. The C14:C16 symmetry  
87 mismatch between the O- and I-layers is accommodated by a unique configuration of two VirB9 and VirB10  
88 subunits; while their NTDs insert in the I-layer, their CTDs do not form part of the O-layer<sup>14</sup> (Figure 2a).  
89 Importantly, the VirB10<sub>CTD</sub> of the O-layer contains a hydrophobic 2-helix bundle (termed the antennae  
90 projection) extending from the VirB10<sub>CTD</sub> β-barrel domains, and 14 of these bundles assemble to form a hollow  
91 pore through the outer membrane. This pore has a diameter of 32 Å at the extracellular entrance, which is  
92 proposed to expand further through a hinge-like conformational change between the antennae projection  
93 helices<sup>14</sup> to accommodate a growing pilus and substrate translocation. This mode of action is in line with earlier  
94 findings that VirB10 associated with the *Agrobacterium tumefaciens* VirB–VirD4 T4SS (T4SS<sub>Agro</sub>) undergoes a  
95 conformational switch in response to sensing and transduction of intracellular signals to gate the outer  
96 membrane channel<sup>22-25</sup>.

97

98 The phytopathogen *Xanthomonas citri* elaborates a T4SS whose constituent subunits are close homologs of  
99 components of the pKM101- and R388-encoded conjugation machines, but this system (T4SS<sub>X. citri</sub>) functions as  
100 an interbacterial killing machine by delivering toxins to neighbouring bacteria<sup>21</sup>. Interestingly, the OMCC of the  
101 T4SS<sub>X. citri</sub> does not display a mismatch between the O- and I- layers as both assume a 14-fold symmetry<sup>21</sup>. It  
102 encodes a much larger VirB7 homologue with a pronounced C-terminal N0 domain<sup>26</sup>, a feature also found in  
103 the Dot/Icm system (T4SS<sub>Dot/Icm</sub>) encoded by *Legionella pneumophila* (see below)<sup>27,28</sup>. The N0 domain widens  
104 horizontally, giving rise to a flying saucer-shaped structure rather than the barrel-like structures of OMCCs from  
105 the T4SS<sub>pKM101</sub> and T4SS<sub>R388</sub> machines. Whether or how these structural variations contribute to the specialized  
106 function of the T4SS<sub>X. citri</sub> machine in interbacterial transmission of toxins is not yet known.

107

108 The nearly intact T4SS<sub>R388</sub> also details the organization of the inner membrane complex (IMC) and periplasmic  
109 stalk (Figure 2a). The stalk connecting the OMCC and IMC has an overall diameter of ~92 Å and length of 216 Å.  
110 The stalk consists of a pentamer of VirB5 subunits located proximally to the OMCC connected to a pentamer of  
111 VirB6 that inserts into the inner membrane by an N-proximal α-helix<sup>14</sup> (Figure 2a). Six knobs (or ‘arches’)  
112 composed of the C-terminal domains of VirB8 subunits surround the central stalk near the inner membrane. The  
113 architecture of the stalk is intriguing in view of prior evidence that the VirB5 subunit localizes at the tip of the T-  
114 pilus elaborated by the *A. tumefaciens* VirB/VirD4 system<sup>29</sup>. Moreover, the finding that the bulk of VirB6 resides  
115 in the periplasm completely revises our views of how VirB6 contributes to substrate translocation and pilus  
116 assembly. VirB6 subunits are highly hydrophobic, and previously were envisioned to adopt a polytopic topology  
117 in the inner membrane and form part of the inner membrane channel<sup>1,30</sup>. In the T4SS<sub>R388</sub> structure, the bulk of  
118 VirB6 is shown to assemble as a pentameric platform entirely in the periplasm while only one N-terminal  
119 hydrophobic domain made of two trans-membrane helices integrates in the inner membrane (Figure 2a). Thus,  
120 most of the hydrophobic domains of VirB6 subunits are shielded from the aqueous environment of the periplasm  
121 through extensive intersubunit contacts. It is also noteworthy that the pentameric symmetry of the VirB5–VirB6  
122 stalk matches that of the conjugative pilus.

123

124 Using structural-complementarity simulations, the VirB2 pilin component of the conjugative pilus was  
125 successfully docked on the VirB6 platform, which led to a new model for how conjugative pili assemble (Figure  
126 2b). Upon synthesis, pilin subunits integrate into the inner membrane, forming a pool for subsequent use in  
127 building the pilus<sup>31</sup> (Figure 2b, step 1). Co-evolution studies confirmed by site-directed mutagenesis identified  
128 one of the two trans-membrane helices as binding and recruitment site for the VirB2 pilin. Upon receipt of an  
129 unknown signal, five pilin subunits are extracted from the inner membrane into the periplasmic assembly site  
130 located in the interacting surfaces of the VirB6 and VirB5 proteins (Figure 2b, step 2). Through reiterative  
131 recruitment and extraction of pilins to the VirB6 platform, the pilus extends and displaces the VirB5 pentamer  
132 upwards and through the outer membrane to the extracellular milieu<sup>14</sup> (Figure 2b, step 3). The VirB5 pentamer  
133 remains at the tip of the pilus, where it binds specific receptors on the target cell surface or embeds directly into  
134 the target cell membrane<sup>32</sup> (Figure 2b, step 4). The role of VirB5 as an adhesin was initially speculated in 2008  
135 (Ref. <sup>31</sup>), and subsequent evidence has been found in the Cag system. In this system, the functional orthologue  
136 of VirB5, termed CagL<sup>33-35</sup>, has been shown to bind integrin on the human cell surface<sup>32</sup>. Furthermore, VirB5 has  
137 exhibited conformational changes similar to those observed in pore-forming proteins<sup>13</sup>, suggesting potential  
138 structural parallels with the translocon pores of type III secretion systems.

139

140 The IMC of the T4SS<sub>R388</sub> is dominated by two concentric rings that extend into the cytoplasm (Figure 2a). These  
141 rings comprise a hexamer of dimers of the VirB4 ATPase<sup>14</sup>. The dimers are arranged so that one protomer forms  
142 the inner ring and the other forms the outer ring. Protomers of each dimer are connected by their NTDs, which  
143 also embed into the inner membrane. Additionally, the NTDs of protomers comprising the inner and outer  
144 hexameric rings form specific contacts with the VirB3 and VirB8 subunits, respectively. This interaction network

145 anchors the VirB4 hexamer of dimers in the inner membrane and potentially enables ATP-dependent structural  
146 changes<sup>14</sup> (Figure 2a).

147

148 Structures of the T4SS<sub>pKM101</sub> and of several mutant machines assembled within the cell envelope also were solved  
149 by *in situ* cryo-ET<sup>36</sup> (Figure 2a). Despite their lower resolutions, these structures revealed several distinctive  
150 features. For example, during assembly of the T4SS<sub>pKM101</sub>, the outer membrane is extensively remodelled as  
151 evidenced by invagination of the outer leaflet and the absence of the inner leaflet of the OM at the machine -  
152 OM junction. The OMCC possesses a central chamber sufficiently large to accommodate a growing pilus as it  
153 extends from the stalk assembly platform. Most importantly, analyses of the IMCs from WT and mutant strains  
154 established that the VirB4 subunit assembles *in vivo* as a central hexamer of dimers at the channel entrance,  
155 and that neither of the VirB11 or VirD4 ATPases contribute to IMC densities<sup>36</sup>. These latter ATPases also were  
156 not visualized in the *in vitro* T4SS<sub>R388</sub> structure, but the VirB11–VirB4 interaction was characterised using  
157 computational methods and validated biochemically and by site-directed mutagenesis. VirB11 and VirD4 might  
158 dock transiently with the VirB channel in response to unknown signals<sup>13</sup>.

159

160

#### 161 [H1] Architectures of expanded systems

162 Expanded T4SSs are composed of up to 25 distinct proteins, encompassing the 12 core components of VirB and  
163 VirD4 along with additional protein subunits<sup>10,11</sup>. The most widely studied expanded systems are the F plasmid-  
164 encoded conjugative machine, and the *L. pneumophila* Dot/Icm and *Helicobacter pylori* Cag effector translocator  
165 systems. Although detailed structures for the IMCs from these systems remain to be determined, near atomic  
166 resolution structures are now available for OMCCs from all three systems, F plasmid-encoded conjugative pili,  
167 and the T4SS<sub>Dot/Icm</sub> substrate recognition platform.

168

169 The OMCC associated with the F system is composed of the three core VirB components, VirB7-like TraV, VirB9-  
170 like TraK and VirB10-like TraB<sup>15,37</sup> (Figures 3a and 3b). It adopts a ‘flying saucer’ shape and is much larger than  
171 the OMCCs of the minimized conjugation machines, with a diameter of ~268 Å and width of 115 Å. The complex  
172 consists of concentric rings termed the outer and inner rings. The inner ring exhibits a 17-fold symmetry and is  
173 composed of seventeen CTDs of TraB and NTDs of TraV. The outer ring displays a 13-fold symmetry and is  
174 composed of 26 CTDs of TraV and 26 copies of TraK (Figure 3a). The TraK subunits assemble as 13 dimers, with  
175 the CTDs of each dimer pair forming 13 elongated knobs that extend radially from the centre of the complex.  
176 The TraB and TraV proteins were observed to form flexible linkers connecting the symmetrically mismatched  
177 inner ring and outer ring. Structural flexibility imparted by the symmetry mismatch could account for the  
178 dynamic properties of the F pilus during extension and retraction. This ability could also be potentiated by a  
179 number of additional proteins present in the expanded F system compared to minimised conjugative systems,  
180 which are not capable of pilus retraction.

181

182 The *L. pneumophila* Dot/Icm and *H. pylori* Cag systems function as effector translocators that aid in infection  
183 processes (Figure 1). The Dot/Icm system has the remarkable capacity to translocate at least 330 effector  
184 proteins, nearly 10 % of the proteome, into eukaryotic cells<sup>28,38,39</sup>. Effector translocation induces a myriad of  
185 physiological changes marked by conversion of human phagosomes into replication-permissive compartments  
186 called *Legionella*-containing vacuoles (LCV)<sup>40</sup>. The OMCC<sub>Dot/Icm</sub> has a highly complex organisation and is  
187 considerably larger (~420 Å in diameter) than that of the F system (Figure 3a). VirB7-like DotD, VirB9-like DotH,  
188 and VirB10-like DotG proteins form the structural scaffold, which is built upon by incorporation of other Dot/Icm-  
189 specific proteins including DotF, DotC, Dis1, Dis2 and Dis3 (Refs. <sup>41,42</sup>). The OMCC<sub>Dot/Icm</sub> has a three-layer topology  
190 with a disk-shaped outer membrane cap (OMC) of 13-fold symmetry, a proximal dome of 16-fold symmetry and  
191 a smaller periplasmic ring of 18-fold symmetry (Figure 3a). Distinct O- and I- layers reminiscent of the OMCC<sub>F</sub>  
192 are likely to be represented by the OMC and PR domains, respectively. In line with this proposal, VirB9-like DotH  
193 was observed to comprise both the OMC and periplasmic ring reminiscent of the architectures of the VirB9  
194 counterparts in the F, pKM101 and R388 systems.

195

196 The Cag system of *H. pylori* secretes the oncoprotein CagA as well as several other nonproteinaceous substrates  
197 into human epithelial cells<sup>43-45</sup> (Figure 1). These T4SS<sub>Cag</sub>-mediated functions induce pathological changes in  
198 epithelial cells that facilitate *H. pylori* infection of the gastrointestinal tract<sup>46</sup>. The T4SS<sub>Dot/Icm</sub> and T4SS<sub>Cag</sub> are the  
199 largest of the T4SSs characterized to date and both possesses some of the structural properties identified in the  
200 other systems. The mushroom-shaped OMCC<sub>Cag</sub> is 400 Å in width and 250 Å in height, and is composed VirB7-  
201 like CagT, VirB9-like CagX and VirB10-like CagY plus two system-specific proteins, Cag3 and CagM<sup>47</sup> (Figure 3a).  
202 The large size of the OMCC<sub>Cag</sub> is conveyed by the larger sizes of CagT, CagX and CagY relative to their VirB  
203 counterparts, and by incorporation of multiple copies of Cag3 and CagM in the structure. The OMCC<sub>Cag</sub> consists  
204 of an OMC with clear O- and I-layers. The OMC is made up of CagT, CagX, CagY, Cag3 and CagM, and the  
205 periplasmic ring composed of CagY and CagX. Portions of the periplasmic ring show structural resemblance to  
206 the I-layer of OMCC<sub>*X. citri*</sub> (Ref. <sup>48</sup>). Both the inner and outer regions of the OMC have a 14-fold symmetry, whereas  
207 the periplasmic ring assumes a 17-fold symmetry (Figure 3a). As shown for other VirB9 subunits, CagX forms  
208 contacts with both the OMC and periplasmic ring, thus bridging the symmetry mismatch between those two  
209 complexes<sup>48</sup>. Reminiscent of the F system, the observed asymmetries among OMCC substructures of the *L.*  
210 *pneumophila* Dot/Icm and *H. pylori* Cag systems might have evolved to confer specialized functions, in these  
211 cases relating specifically to the infection process. OMCC structural flexibility might, for example, be needed to  
212 establish dynamic yet productive contacts with eukaryotic host cells or to coordinate the timing and delivery of  
213 substrates into the eukaryotic cell targets.

214

215 These expanded T4SSs also have been visualized by *in situ* cryo-ET in their native cellular contexts. Remarkably,  
216 F systems elaborate a presumptively quiescent translocation channel and three morphologically distinct  
217 platforms upon which the F pilus is docked<sup>49</sup> (Figure 3b). The channel, designated as the F1-channel complex,  
218 consists of the OMCC joined to the IMC by a periplasmic cylinder that is thicker and more pronounced than the  
219 thin periplasmic stalk of the T4SS<sub>R388</sub> (Figure 3b). The central hexamer of dimer configuration of the VirB4-like



220 TraC ATPase is readily visualized at the cytoplasmic entrance, reminiscent of the *in situ* T4SS<sub>pKM101</sub> and recent *in*  
221 *vitro* high resolution T4SS<sub>R388</sub> structures (Figure 2a). An F-pilus associated structure, termed the F2–channel–  
222 pilus complex, resembles the F1 complex but has the F pilus attached at the distal end of the OMCC (Figure 3b).  
223 The F1 and F2 complexes are postulated to correspond to the quiescent channel and active pilus-assembly  
224 factory involved in mate-seeking and mating. Two other F pilus-associated structures, designated as the F3–talk–  
225 pilus and F4–outer membrane-pilus complexes, consist of the F pilus attached respectively to a thin stalk density  
226 that spans the periplasm or a small outer membrane density without any underlying structure. The F3 and F4  
227 complexes lack discernible channels for substrate transfer or pilus assembly, and accordingly are proposed to  
228 function exclusively as holding platforms for nonretractile F pili. These inert structures might contribute to  
229 nonspecific cell aggregation and biofilm formation or as decoys for bacteriophages that rely on F pilus retraction  
230 to gain access to the cell envelope<sup>49</sup>.

231  
232 Visualization of the *in situ* T4SS<sub>Dot/Icm</sub> structure revealed an OMCC with a ‘Wi-Fi symbol’-like architecture of 400  
233 Å in diameter whose assembly is dependent on the DotC, DotD, DotF, DotG and DotH subunits<sup>50,51</sup> (Figure 3c).  
234 The OMCC is connected to a cylinder with an outer diameter of ~20nm and a central lumen or channel of ~6 nm,  
235 which narrows to a diameter of ~10nm and a channel of ~3nm near the IM<sup>51</sup>. As with other T4SSs (Refs. 14,21,36),  
236 at the cytoplasmic face of the IMC is the hexamer of dimer configuration of VirB4 ATPase (DotO). Remarkably,  
237 VirB11-like DotB, a second ATPase of this system, assembles as a hexamer that dynamically associates with the  
238 DotO inner hexamer by a mechanism dependent on cycles of ATP binding and hydrolysis (see below)<sup>51</sup>. Recently,  
239 another Dot/Icm system elaborated by *Coxiella burnetii* has been determined by a combination of cryo-ET and  
240 cryo-focused ion beam (cryo-FIB) milling to closely resemble that of *L. pneumophila*<sup>52</sup>. Interestingly, this study  
241 documented a correlation between assembly of the machinery and developmental transitions of *C. burnetii*  
242 cells during infection, which complements previous observations that reported a dependence of effector  
243 translocation by this T4SS on the progression of *C. burnetii* infection<sup>53</sup>.

244  
245 In the *in situ* cryo-ET map of the *H. pylori* Cag machine, the OMCC resembles the equivalent substructure solved  
246 at a higher resolution by cryo-EM<sup>48,54-56</sup>. Analyses of mutant machines confirmed that *in situ* assembly of the  
247 OMCC requires the Cag subunits CagX, CagY and CagM, and that CagT and Cag3 contribute to peripheral  
248 densities. Other noteworthy features of the *in situ* T4SS<sub>Cag</sub> machine include a hollow cylinder that extends across  
249 the periplasm, connecting the OMCC to the IMC. The IMC is architecturally more complex than the equivalent  
250 substructures of the F and Dot/Icm systems in having three concentric rings instead of two. A unique feature  
251 among T4SSs is that the extracellular domain of the CagY subunit of the T4SS<sub>Cag</sub> contains multiple binding sites  
252 for Toll-like receptor 5 (TLR5) and functions in regulating immune responses of the host<sup>57</sup>. The inner and middle  
253 rings correspond to the central and outer hexamers of VirB4-like CagE, but assembly of the outer ring is  
254 dependent on production of VirD4-like Cagβ<sup>55</sup>. VirB11-like Cagα associates at the base of the CagE central  
255 hexamer, but in contrast to the Dot/Icm system, Cagα seems to associate stably with CagE and not dynamically  
256 as a function of ATP binding and hydrolysis as shown for DotB<sup>55</sup> (Figure 3d). A comprehensive table that

257 summarises all available structures to date comprising both, the minimised and expanded systems is provided  
258 as Supplementary Table 1.

259

260

### 261 **[H1] Other T4SS machine adaptations**

262 Besides appropriating novel subunits for functional diversification, many T4SSs of both the minimised and  
263 expanded types have diversified through modifications of core VirB components. VirB2-like pilins or pili or  
264 associated surface adhesins have been adapted to enhance T4SS targeting to specific cell types (see below),  
265 whereas certain IMC or OMCC components have undergone modifications through acquisition of novel domains  
266 for broadened T4SS functionality (Figure 4). These modifications generally function to direct machine assembly  
267 at specific sites within the cell or coordinate T4SS localization or function with the cell cycle, or to promote  
268 attachment to specific target cells, as described in more detail in supplementary text box 1. Symmetry  
269 mismatches are likely to provide regions of mobility or flexibility between different protein complex layers or  
270 subassemblies. However, despite the presence of symmetry mismatch in several types of secretion systems,  
271 precisely how symmetry mismatch contributes to machine functions at mechanistic or structural levels have not  
272 been established for any characterized secretion system <sup>10</sup>.

273

274 The VirB6 subunits are the most extensively modified of the IMC components. In many T4SSs, VirB6 subunits are  
275 composed predominantly of 5-7 hydrophobic domains that are likely to assemble as part of the central stalk  
276 structure, as demonstrated for the R388-encoded VirB6 subunit (Figure 1a). However, many VirB6 subunits  
277 termed 'extended-VirB6s' are considerably larger by virtue of the presence of one or more large central of C-  
278 terminal hydrophilic domains<sup>1</sup> (Figure 4). Remarkably, where characterized these hydrophilic domains  
279 contribute in distinct ways to establishment or inhibition of productive donor–target cell interactions. In F  
280 systems, a large ~600 residue C-terminal hydrophilic domain (CTD) of VirB6-like TraG is involved in entry  
281 exclusion, a process that blocks redundant DNA transfer between the donor cells. When donor cells form mating  
282 junctions with other donor cells, the CTD of TraG produced by one donor cell establishes contact with TraS<sub>F</sub>, an  
283 inner membrane protein produced by the paired donor cell <sup>58,59</sup>. This contact is achieved either by extension of  
284 TraG<sub>F</sub> across the mating junction or by proteolytic cleavage and translocation of the CTD of TraG<sub>F</sub> through the  
285 T4SS<sub>F</sub> into the paired donor cell. In *Rickettsia spp.*, multiple copies of extended-VirB6s are present with sizes  
286 ranging from 600 to over 1400 residues <sup>60,61</sup>. Large hydrophilic domains are surface displayed where they are  
287 implicated in promoting endosymbiotic or pathogenic relationships with eukaryotic target cells<sup>62</sup>. In the *L.*  
288 *pneumophila* Dot/Icm system, VirB6-like DotA possesses multiple hydrophobic domains flanking a central  
289 hydrophilic domain. Although DotA associates with the inner membrane reminiscent of other VirB6 family  
290 members, it can also be exported in a Dot/Icm T4SS-dependent manner to the extracellular milieu where it forms  
291 ring-like oligomers whose functions are presently unknown <sup>63</sup>.

292

293 All three of the core VirB components of OMCCs can be modified through acquisition of novel motifs (Figure 4).

294 Although many VirB7-like lipoproteins are small (~50 residues) and resemble the archetypal *A. tumefaciens*

295 VirB7, many others are considerably larger (~160-300 residues) as shown for *H. pylori* CagT, *X. citri* VirB7 and *L.*  
296 *pneumophila* DotD<sup>11,21,41,48</sup>. In the *H. pylori* system, both CagX and CagY are considerably larger than their VirB9  
297 and VirB10 counterparts. Indeed, in the case of CagY, only the extreme C-terminal region adopts the  
298 characteristic VirB10  $\beta$ -barrel-domain folds that assemble as the central rings of OMCCs. A large middle repeat  
299 region (MRR) is composed of multiple repeats, which undergo extensive rearrangement during gene expression.  
300 These rearrangements yield many CagY variants that have been shown to regulate T4SS<sub>Cag</sub> function — positively  
301 or negatively — to maximize persistent infection<sup>64-66</sup>.

302

303

#### 304 **[H1] VirD4 substrate recruitment and translocation**

305 For most T4SSs, VirD4-like ATPases also known as type IV coupling proteins (T4CPs)<sup>22,23,67</sup> are responsible for  
306 substrate recruitment. T4CPs characteristically possess an N-terminal transmembrane domain (TMD) implicated  
307 in establishment of contacts with IMC components of cognate T4SSs. A conserved nucleotide-binding domain  
308 (NBD) is thought to provide the energy for early-stage substrate processing; for example, unfolding and opening  
309 of the channel for substrate transfer. Two sequence-variable domains, the all-alpha domain (AAD) and C-  
310 terminal domain (CTD) if present, contribute to substrate recruitment. An X-ray structure of R388-encoded  
311 TrwB, currently the structural archetype for T4CPs, showed that the NBD assembles as a homohexamer<sup>68</sup> (Figure  
312 5a). This NBD architecture bears similarities to the FtsK and SpoIIIE families of DNA motor proteins involved in  
313 DNA translocation during cytokinesis<sup>67</sup>. The AAD sits at the base of the hexamer, optimally positioned for  
314 docking of secretion substrates. Indeed, evidence has now been presented for binding of AADs to secretion  
315 substrates in the *A. tumefaciens* and *Xanthomonas* VirB–VirD4 systems<sup>69,70</sup>. Protein substrates are recognised  
316 by the T4SS through conserved motifs called translocation signals. These highly specific signals encoded by the  
317 protein substrates are tailored for the timely engagement and controlled secretion by the T4S apparatus. Details  
318 on the different translocation signals associated with T4SS substrates can be found in the supplementary text  
319 box 2.

320

321 VirD4 homologues also interact with VirB11 ATPases<sup>22,71,72</sup>. VirB11 family members are structurally similar  
322 (Figure 5b) insofar as their NTDs and CTDs resemble each other and are connected by a flexible linker. VirB11  
323 subunits assemble as homohexamers<sup>73</sup>, and in this oligomeric state, the interdomain linkers facilitate fluent  
324 domain swaps without affecting hexamer assembly<sup>74</sup>. The VirB11, VirD4 and VirB4 ATPases act in concert to  
325 orchestrate pilus biogenesis and substrate transfer, although mechanistic details underlying this coordination of  
326 ATPase functions remain unknown<sup>22,71,72,75,76</sup>. The VirB11 ATPases are viable drug targets, as illustrated by an  
327 early report that small molecule inhibitors of VirB11-like Cag $\alpha$  blocks virulence of *H. pylori*<sup>77</sup>.

328

329 In the *L. pneumophila* Dot/Icm system, the CTD of VirD4-like DotL has a highly complex role in recruitment of its  
330 many protein effectors and their subsequent secretion through the T4SS<sub>Dot/Icm</sub> apparatus (Figure 5c). Although  
331 recruitment of various effectors to DotL can proceed independently of known associated chaperones,  
332 recruitment of others is strictly dependent on the IcmS and IcmW chaperones, with or without an additional

333 requirement for the LvgA chaperone<sup>78-81</sup>. DotL assembles as a hexamer, and associated with each of the six CTDs  
334 are various Dot adaptors including DotM, DotN, DotY, DotZ, IcmS and IcmW. The DotM adaptor itself also acts  
335 as a recruitment platform for the some of the IcmSW-independent effectors<sup>82</sup>. The six CTD-adaptor complexes  
336 together form a bell-shaped structure, termed the type IV coupling complex (T4CC), that extends into the  
337 cytoplasm and functions as the substrate recruitment platform (Figure 5c). The T4CC possesses at least two  
338 known effector binding-sites, one on DotM and a second strictly dependent on the IcmS and IcmW chaperones,  
339 with or without an additional requirement for the LvgA chaperone<sup>78-81</sup>. Through binding of distinct arrays of  
340 effectors based on their associations with different chaperones, the T4CC is envisioned to regulate substrate  
341 transfer during *L. pneumophila* infection<sup>83-88</sup>.

342

343 In the *H. pylori* Cag T4SS, VirD4-like Cag $\beta$  is structurally similar to TrwB (Figure 5a); however its AAD contributes  
344 in a unique way to modulation of Cag $\beta$  function. In this system, two cytosolic proteins, CagF and CagZ, function  
345 together with Cag $\beta$  to recruit the CagA substrate to the T4SS<sub>cag</sub>. Prior work showed that CagF functions as a  
346 chaperone by binding a 100-residue region of CagA, whereas CagZ stabilizes Cag $\beta$ <sup>89</sup>. Recently, crystal structures  
347 presented for the Cag $\beta$  AAD–CagZ interaction led to a model whereby the CagZ–AAD contact maintains Cag $\beta$  in  
348 a monomeric state, thereby suppressing ATPase activity and rendering Cag $\beta$  inactive<sup>90</sup>. Upon receipt of an  
349 unknown signal, CagF binds and recruits CagA to Cag $\beta$ , resulting in release of CagZ and assembly of the Cag $\beta$   
350 hexamer. This catalytically active form of Cag $\beta$  then unfolds and translocates CagA through the T4SS<sub>cag</sub>.

351

352 Among the conjugative T4SSs, T4CPs recruit a specialised DNA-processing complex called the relaxosome<sup>5,91</sup>  
353 (Figure 6a). In the well-characterized F system, the relaxosome is composed of four proteins assembled at the  
354 origin-of-transfer (*oriT*) sequence of the F plasmid. The largest relaxosome subunit, Tral relaxase (~200 kDa),  
355 possesses a trans-esterase domain that nicks and covalently attaches to the 5' end of the nicked DNA strand  
356 destined for translocation (T-strand). Tral also possesses a vestigial helicase domain that serves as a single-  
357 stranded DNA (ssDNA)-binding domain, an active 5' to 3' helicase domain, and a C-terminal domain that  
358 functions as a recruitment platform for the remaining relaxosome components<sup>92,93</sup>. Two other relaxosome  
359 components TraY and IHF cause conformational changes in the DNA topology that expose the nick (*nic*) site for  
360 cleavage by Tral.<sup>94,95</sup> Finally, TraM is a homotetramer responsible for docking the DNA–relaxosome complex to  
361 the coupling protein TraD<sup>96,97</sup> (Figure 6a). On the DNA side, a pair of TraM tetramers recognise a particular DNA  
362 sequence known as *sbmABC* motifs within the *oriT* of the F-plasmid<sup>98</sup>, resulting in up to six tetramers bound to  
363 one F plasmid. Each TraM tetramer is subsequently recognised by C-terminal tails of the hexameric TraD<sup>96</sup> (Figure  
364 6a). This interaction ensures F plasmid docking and transfer while actively blocking translocation of a co-existing  
365 conjugative plasmid(s) through the F machine<sup>84,97,98</sup>.

366

367 Remarkably, at this time there is little detailed structural information concerning the physical relationship  
368 between the T4CP and the T4SS channel. Consequently, the route or routes by which DNA and protein substrates  
369 are conveyed through T4SSs is not known, and two distinct translocation pathways have been envisioned (Figure  
370 6). As illustrated for the T4SS<sub>dot/lcm</sub> machine, upon recruitment of substrates to the DotL T4CC, the T4CC functions

371 in one of two ways, which ultimately dictates whether substrates are delivered in one or two steps across the  
372 entire cell envelope (Figure 6B). In the one-step translocation pathway<sup>99</sup>, DotL is situated beneath or near the  
373 T4SS and, upon substrate engagement, the T4CC passes captured substrates to the base of the T4SS channel  
374 marked by the DotB and DotO hexameric ATPases. The DotL–DotB–DotO ATPase ternary complex then  
375 orchestrates substrate unfolding, dissociation of chaperones and/or adaptors, and delivery of the translocation  
376 intermediate into the channel for conveyance in one step through a channel that extends from the cytoplasmic  
377 face of the inner membrane to the cell exterior (Figure 6b). In the alternative two-step translocation model<sup>99</sup>,  
378 DotL is situated in physical proximity to the T4SS. The T4CC captures and then shunts substrates directly into the  
379 lumen of the DotL hexamer (whose NTD spans the inner membrane) for delivery across the inner membrane.  
380 Once in the periplasm, in a second translocation reaction, substrates are recruited to and enter the T4SS channel  
381 for delivery to the cell surface<sup>83,51,100</sup> (Figure 6b). For reasons outlined in the next paragraph, we hypothesize  
382 that delivery of the F plasmid transfer intermediate follows the one-step pathway, whereby TraD docks at the  
383 base of the channel in complex with VirB4-like TraC<sup>84</sup> (Figure 6a).

384

385 In the absence of detailed structural information about the T4CP–T4SS connection, we currently favor the one-  
386 step pathway for DNA as well as protein substrates, given the potentially deleterious consequences  
387 (degradation, misfolding, misrouting and temporal disruption) encountered by ssDNA transfer intermediates or  
388 as many as several hundred effectors delivered into the bacterial periplasm via the two-step pathway. Early  
389 crosslinking studies in *A. tumefaciens* system also supplied experimental support for a one-step pathway. In  
390 those studies, DNA substrates of the VirB–VirD4 system were shown to engage in sequential order with ATPase  
391 subunits comprising the cytoplasm–inner membrane interface, then with components of the IMC, and finally  
392 with components of the OMCC and pilus<sup>22,23,30,71,101</sup>. Structural studies of the T4SS<sub>R388</sub> by negative stain-EM<sup>102</sup>  
393 and of the T4SS<sub>Cag</sub> by *in situ* cryo-ET<sup>49</sup> also have supplied evidence that T4CPs can associate with the VirB4  
394 hexameric platform at the channel entrance, thus being optimally positioned to deliver captured substrates  
395 directly into the channel. While there are clear examples of T4SSs that utilize two-step translocation pathways  
396 to deliver substrates to the extracellular milieu<sup>103</sup> or to eukaryotic target cells<sup>104</sup>, these systems lack VirD4 T4CPs  
397 and thus rely on alternative secretion systems for recruitment and translocation of substrates across the inner  
398 membrane.

399

400

#### 401 [H1] Conjugative pili and target cell attachment

402 T4SSs elaborate various surface structures that have important roles in promoting donor–target cell contacts.  
403 Among these, conjugative pili are major contributors to the rapid and widespread dissemination of plasmids and  
404 other mobile elements, and their cargoes of antibiotic resistance determinants, among Gram-negative bacteria.  
405 High-resolution structures recently have been generated for several conjugative pili, including those produced  
406 by F plasmids (F pilus)<sup>105,106</sup>, the *A. tumefaciens* VirB–VirD4 system (T pilus)<sup>107-109</sup> and IncN plasmid pKM101<sup>108</sup>.  
407 Throughout evolution, the relationships between hosts and pathogens have led to adaptations in T4SS-  
408 associated pili, resulting in more specialized functions. Using a ‘one-size-fits-all’ approach is not effective for

409 adhesion to distinct host-encoded receptors or different biotic and abiotic surfaces. As a result, pili and pilins  
410 have diversified to fulfil these functions. The supplementary text box 3 summarizes the diversification of pili and  
411 bacterial adhesins and their role in establishing close contacts with target cells.

412

413 Structurally, assembled pili differ in rotational raise of subunits (Figure 7a) and can display either a five-start  
414 helical symmetry, as shown for T- and N-pili and F-pili encoded by the classical F plasmid and F-like pED208, or  
415 a one-start symmetry as shown for another F-pilus encoded by pKpQIL or an Archaeal conjugative pilus<sup>109</sup>. The  
416 outer diameters of conjugative pili in Gram-negative species are 76 Å - 87 Å and inner lumens are 23 Å - 26 Å in  
417 width, whereas the archaeal pilus has an inner diameter of 16 Å (Figure 7b).

418

419 As noted earlier, pilin subunits accumulate in the inner membrane as a pool for recruitment to build the  
420 conjugative pilus upon receipt of an unknown signal. Intriguingly, structural studies of the conjugative pili have  
421 established that, during extraction from the inner membrane, pilins co-extract phospholipid molecules. In F  
422 systems, for example, TraA pilins co-extract phosphatidylglycerol molecules in a 1:1 stoichiometry (Figure 7C),  
423 resulting in assembly of the helical fiber with phosphatidylglycerol molecules lining the pilus lumen. These  
424 phosphatidylglycerol molecules impart an overall negative charge to the F pilus lumens<sup>105,106</sup>. The *A. tumefaciens*  
425 T pilus<sup>108,109</sup> and pKM101-encoded N pilus<sup>108</sup> share the general features first reported for F pili, but the lumens  
426 are lined with phospholipids with different head groups (Figure 7c). For N pili this results in an overall negative  
427 charge reminiscent of F pili<sup>108</sup>, but for T pili the lumen has an overall positive charge. Another interesting  
428 difference is the presence of a kink between the first alpha helices of pilins comprising the T- and N- pili, which  
429 is absent in pilins associated with pili from expanded systems (Figure 7c; arrow). Why conjugative pili differ in  
430 phospholipid compositions and what is the significance of the kink between helices  $\alpha 1$  and  $\alpha 2$  is unknown, but  
431 it is reasonable to propose that these features impart biophysical properties of importance for specialized  
432 functions in different environmental conditions.

433

434 In support of this model, recent biophysical studies have demonstrated that F pili are extremely flexible and  
435 have spring-like properties with pronounced structural and thermochemical robustness. These properties are  
436 postulated to accelerate conjugation rates and biofilm formation by F-plasmid-carrying cells by allowing for  
437 effective function even in highly turbulent environments, such as those present in human gastrointestinal tracts  
438 <sup>110</sup>. This unique feature of F-pili might well be responsible for recent evidence that IncF plasmids are the most  
439 dominant types of conjugative plasmids present in enterobacterial isolates from humans and animals <sup>111</sup>. In  
440 contrast to F pili, other conjugative pili are generally shorter and more rigid and have not been shown to  
441 retract<sup>112</sup>. Because of their distinctive biophysical properties, these rigid pili are envisioned to readily break from  
442 the cell surface, accumulate in the milieu, and mediate nonspecific aggregation of donor and potential recipient  
443 cells, thus acting indirectly to facilitate propagation of mobile elements.

444

445

446 **[H1] Conclusions and outlook**

447 The remarkable recent progress in defining the architectures of T4SSs, both *in vitro* and *in situ*, confirms that the  
448 functional diversity of these fascinating nanomachines is recapitulated at the structural level. Although there  
449 clearly are emergent structural themes, most if not all T4SSs also have acquired systems-specific properties. This  
450 is particularly evident with the expanded systems, which have appropriated components from unknown  
451 ancestries that physically enlarge and add structural complexity to the T4SSs. The contribution of T4SS structural  
452 diversity to their varied functions is still not fully understood. However, it is possible to speculate on potential  
453 relationships. For instance, differences in pilin or adhesin subunits may result in variations in pilus biogenesis,  
454 assembly and adherence properties. Another factor to consider is cargo recruitment, where structural  
455 differences in the T4CP receptor or complex are likely to have evolved to specify restricted or expanded  
456 substrate repertoires. Additionally, T4SS diversity at both the structural and functional levels are likely to have  
457 evolved for recognition of specific host cell receptors, ultimately dictating the range of hosts that the T4SS can  
458 target. Interestingly, DNA and protein substrates also have evolved a bewildering array of translocation signals  
459 (supplementary text box 2), along with deployment of chaperones or adaptors, for docking with VirD4 substrate  
460 recruitment platforms. In conjunction, VirD4 evolved to carry sequence-variable motifs or domains (for example,  
461 AAD, CTD and T4CC) to specify and temporally regulate loading and delivery of substrates into the translocation  
462 channel.

463

464 The T4SS field is well-poised to answer several long-standing questions. Most importantly, we still lack critical  
465 information about the physical and functional relationship of the VirD4 T4CP with the cognate T4SS channel.  
466 Also, what constitutes the translocation channel across the periplasm and the route of substrate transfer across  
467 the entire cell envelope? At the cell exterior, how do mating junctions form, how are they physically configured,  
468 and how do they dissociate after substrate transfer is completed? To what extent or for which systems do  
469 conjugative pili routinely transmit DNA and protein substrates through their lumens? To address these  
470 questions, a combination of structural analyses of mutant machines, fixed in their activated states or actively  
471 engaged in substrate transfer, and other approaches such as correlative light and electron microscopy (CLEM)  
472 offer considerable promise. Finally, and most central to this Review, how do the various T4SS structural  
473 adaptations confer system-specific functions? A full answer to this question will be generated by widening the  
474 current subjects of study to include the many other T4SSs functioning in diverse species of bacteria and archaea.

475

476 There is growing interest in translational initiatives aimed at blocking or repurposing T4SSs for therapeutic ends.  
477 High-throughput screens are being used to identify small-molecule inhibitors, with goals of blocking conjugative  
478 dissemination of antibiotic resistance or inhibiting effector translocation to suppress pathogenesis<sup>6,7,113-120</sup>.  
479 Structural advances of the different T4SSs summarized in this Review will continue to facilitate the rational  
480 design of small molecules effective at blocking critical subunit–subunit interfaces. Conversely, as T4SSs are the  
481 only bacterial secretion systems capable of delivering DNA or protein substrates to a wide range of target cell  
482 types, these nanomachines are excellent delivery systems for therapeutic interventions. Indeed, the early  
483 discovery of *A. tumefaciens*-mediated T-DNA transfer, along with the realization that any DNA of interest can be  
484 substituted for oncogenic T-DNA, spawned an entirely new field of plant genetic engineering<sup>121</sup>. In recent years,

485 conjugation machines have been repurposed to deliver CRISPR–Cas9 systems to bacterial recipients to cure drug  
486 resistance plasmids or kill recipient cells harbouring CRISPR–Cas9 target sequences <sup>122-125</sup>. Very recently,  
487 bacterial donors engineered to surface display nanobodies were shown to selectively deliver DNA cargoes to  
488 recipient cells displaying the cognate antigens <sup>126</sup>. These types of translational advances set the stage for  
489 deployment of T4SSs for selective killing of bacterial targets or even of cancer cells.

490

491 In the 20 years since the state of knowledge of the fascinatingly versatile T4SSs was first reviewed<sup>2</sup>, the field has  
492 made astounding progress in defining many T4SS structures and mechanisms of actions, and identifying the  
493 range of cellular consequences accompanying effector translocation. We fully expect the next 20 years to yield  
494 even more exciting fundamental and translational advances.

495

496

#### 497 **Acknowledgements**

498 Work in the authors' laboratories was supported by the Wellcome Trust grants 215164/Z/18/Z and  
499 217089/Z/19/Z to T.R.D.C. and G.W., respectively, and National Institutes of Health grants NIH 1R35GM131892  
500 and NIH 1R21AI159970 to P.J.C.

501

#### 502 **Author contributions**

503 T.R.D.C, J.B.P. and P.J.C. wrote the article. T.R.D.C., J.B.P., P.J.C. and K.M. researched data for the article. K.M.  
504 made figures and table with contributions from T.R.D.C. and J.B.P. All authors reviewed and/or edited the  
505 manuscript before submission.

506

#### 507 **Competing interests**

508 The authors declare no competing interests.

509

#### 510 **Supplementary information**

511 Supplementary information is available for this paper at <https://doi.org/10.1038/s415XX-XXX-XXXX-X>

512



513 **References**

514

- 515 1 Alvarez-Martinez, C. E. & Christie, P. J. Biological diversity of prokaryotic type IV secretion systems.  
516 *Microbiology and Molecular Biology Reviews* **73**, 775-808 (2009).
- 517 2 Cascales, E. & Christie, P. J. The versatile bacterial type IV secretion systems. *Nature Reviews*  
518 *Microbiology* **1**, 137-149 (2003). <https://doi.org/10.1038/nrmicro753>
- 519 3 Costa, T. R. *et al.* Secretion systems in Gram-negative bacteria: structural and mechanistic insights. *Nat*  
520 *Rev Microbiol* **13**, 343-359 (2015). <https://doi.org/10.1038/nrmicro3456>
- 521 4 Christie, P. J. The Mosaic Type IV Secretion Systems. *EcoSal Plus* **7** (2016).  
522 <https://doi.org/10.1128/ecosalplus.ESP-0020-2015>
- 523 5 Waksman, G. From conjugation to T4S systems in Gram-negative bacteria: a mechanistic biology  
524 perspective. *EMBO Rep* **20** (2019). <https://doi.org/10.15252/embr.201847012>
- 525 6 Cabezon, E., de la Cruz, F. & Arechaga, I. Conjugation Inhibitors and Their Potential Use to Prevent  
526 Dissemination of Antibiotic Resistance Genes in Bacteria. *Front Microbiol* **8**, 2329 (2017).  
527 <https://doi.org/10.3389/fmicb.2017.02329>
- 528 7 Boudaher, E. & Shaffer, C. L. Inhibiting bacterial secretion systems in the fight against antibiotic  
529 resistance. *Medchemcomm* **10**, 682-692 (2019). <https://doi.org/10.1039/c9md00076c>
- 530 8 Christie, P. J., Atmakuri, K., Krishnamoorthy, V., Jakubowski, S. & Cascales, E. Biogenesis, architecture,  
531 and function of bacterial type IV secretion systems. *Annu Rev Microbiol* **59**, 451-485 (2005).  
532 <https://doi.org/10.1146/annurev.micro.58.030603.123630>
- 533 9 Cabezón, E., Ripoll-Rozada, J., Peña, A., de la Cruz, F. & Arechaga, I. Towards an integrated model of  
534 bacterial conjugation. *FEMS Microbiol Rev* **39**, 81-95 (2015). <https://doi.org/10.1111/1574-6976.12085>
- 535 10 Costa, T. R. D. *et al.* Type IV secretion systems: Advances in structure, function, and activation. *Mol*  
536 *Microbiol* **115**, 436-452 (2021). <https://doi.org/10.1111/mmi.14670>
- 537 11 Sheedlo, M. J., Ohi, M. D., Lacy, D. B. & Cover, T. L. Molecular architecture of bacterial type IV secretion  
538 systems. *PLoS Pathog* **18**, e1010720 (2022). <https://doi.org/10.1371/journal.ppat.1010720>
- 539 12 Sgro, G. G. *et al.* Bacteria-Killing Type IV Secretion Systems. *Front Microbiol* **10**, 1078 (2019).  
540 <https://doi.org/10.3389/fmicb.2019.01078>
- 541 13 Gonzalez-Rivera, C., Bhatti, M. & Christie, P. J. Mechanism and Function of Type IV Secretion During  
542 Infection of the Human Host. *Microbiol Spectr* **4** (2016). <https://doi.org/10.1128/microbiolspec.VMBF-0024-2015>
- 543
- 544 14 Macé, K. *et al.* Cryo-EM structure of a type IV secretion system. *Nature* **607**, 191-196 (2022).  
545 <https://doi.org/10.1038/s41586-022-04859-y>
- 546 **The first high-resolution atomic structure of a nearly complete T4SS representing a significant leap**  
547 **forward in the understanding of type IV secretion, as it reveals crucial details of assembly, function,**  
548 **and subunit interfaces, opening new possibilities for rational drug design and establishing a workflow**  
549 **for structural determination of these complex machineries.**
- 550 15 Amin, H., Ilangovan, A. & Costa, T. R. D. Architecture of the outer-membrane core complex from a  
551 conjugative type IV secretion system. *Nature Communications* **12**, 6834 (2021).  
552 <https://doi.org/10.1038/s41467-021-27178-8>
- 553 **The first high-resolution structure of the outer membrane core complex from an expanded**  
554 **conjugative T4SS shedding light on the mechanisms of conjugative pilus outgrowth and DNA**  
555 **translocation during bacterial conjugation, revealing structural adaptations that contribute to the**  
556 **dynamic properties of the machinery.**
- 557 16 Chandran, V. *et al.* Structure of the outer membrane complex of a type IV secretion system. *Nature*  
558 **462**, 1011-1015 (2009). <https://doi.org/10.1038/nature08588>

- 559 17 Fronzes, R. *et al.* Structure of a Type IV Secretion System Core Complex. *Science* **323**, 266-268 (2009).  
560 <https://doi.org/doi:10.1126/science.1166101>
- 561 18 Rivera-Calzada, A. *et al.* Structure of a bacterial type IV secretion core complex at subnanometre  
562 resolution. *The EMBO Journal* **32**, 1195-1204 (2013).  
563 <https://doi.org/https://doi.org/10.1038/emboj.2013.58>
- 564 19 Low, H. H. *et al.* Structure of a type IV secretion system. *Nature* **508**, 550-553 (2014).  
565 <https://doi.org/10.1038/nature13081>
- 566 20 Gordon, J. E. *et al.* Use of chimeric type IV secretion systems to define contributions of outer membrane  
567 subassemblies for contact-dependent translocation. *Mol Microbiol* **105**, 273-293 (2017).  
568 <https://doi.org/10.1111/mmi.13700>
- 569 21 Sgro, G. G. *et al.* Cryo-EM structure of the bacteria-killing type IV secretion system core complex from  
570 *Xanthomonas citri*. *Nat Microbiol* **3**, 1429-1440 (2018). <https://doi.org/10.1038/s41564-018-0262-z>
- 571 **The paper reports the high-resolution cryo-EM structure of a T4SS involved in bacterial killing**  
572 **advancing our understanding of the structural similarities and differences among functionally distinct**  
573 **T4SSs.**
- 574 22 Cascales, E., Atmakuri, K., Sarkar, M. K. & Christie, P. J. DNA Substrate-Induced Activation of the  
575 *Agrobacterium* VirB/VirD4 Type IV Secretion System. *Journal of Bacteriology* **195**, 2691-2704 (2013).  
576 <https://doi.org/doi:10.1128/JB.00114-13>
- 577 23 Cascales, E. & Christie, P. J. *Agrobacterium* VirB10, an ATP energy sensor required for type IV  
578 secretion. *Proceedings of the National Academy of Sciences* **101**, 17228-17233 (2004).  
579 <https://doi.org/doi:10.1073/pnas.0405843101>
- 580 24 Banta, L. M. *et al.* An *Agrobacterium* VirB10 Mutation Conferring a Type IV Secretion System Gating  
581 Defect. *Journal of Bacteriology* **193**, 2566-2574 (2011). <https://doi.org/doi:10.1128/JB.00038-11>
- 582 25 Darbari, V. C. *et al.* Electrostatic Switching Controls Channel Dynamics of the Sensor Protein VirB10 in  
583 *A. tumefaciens* Type IV Secretion System. *ACS Omega* **5**, 3271-3281 (2020).  
584 <https://doi.org/10.1021/acsomega.9b03313>
- 585 26 Souza, D. P. *et al.* A Component of the Xanthomonadaceae Type IV Secretion System Combines a VirB7  
586 Motif with a NO Domain Found in Outer Membrane Transport Proteins. *PLOS Pathogens* **7**, e1002031  
587 (2011). <https://doi.org/10.1371/journal.ppat.1002031>
- 588 27 Nakano, N., Kubori, T., Kinoshita, M., Imada, K. & Nagai, H. Crystal Structure of Legionella DotD: Insights  
589 into the Relationship between Type IVB and Type II/III Secretion Systems. *PLOS Pathogens* **6**, e1001129  
590 (2010). <https://doi.org/10.1371/journal.ppat.1001129>
- 591 28 Lockwood, D. C., Amin, H., Costa, T. R. D. & Schroeder, G. N. The Legionella pneumophila Dot/Icm type  
592 IV secretion system and its effectors. *Microbiology (Reading)* **168** (2022).  
593 <https://doi.org/10.1099/mic.0.001187>
- 594 29 Aly, K. A. & Baron, C. The VirB5 protein localizes to the T-pilus tips in *Agrobacterium tumefaciens*.  
595 *Microbiology* **153**, 3766-3775 (2007). <https://doi.org/10.1099/mic.0.2007/010462-0>
- 596 30 Jakubowski, S. J., Krishnamoorthy, V., Cascales, E. & Christie, P. J. *Agrobacterium tumefaciens* VirB6  
597 domains direct the ordered export of a DNA substrate through a type IV secretion System. *Journal of*  
598 *molecular biology* **341**, 961-977 (2004). <https://doi.org/10.1016/j.jmb.2004.06.052>
- 599 31 Hospenthal, M. K., Costa, T. R. D. & Waksman, G. A comprehensive guide to pilus biogenesis in Gram-  
600 negative bacteria. *Nature Reviews Microbiology* **15**, 365-379 (2017).  
601 <https://doi.org/10.1038/nrmicro.2017.40>
- 602 32 Aly, K. A. & Baron, C. The VirB5 protein localizes to the T-pilus tips in *Agrobacterium tumefaciens*.  
603 *Microbiology* **153**, 3766-3775 (2007). <https://doi.org/https://doi.org/10.1099/mic.0.2007/010462-0>
- 604 33 Backert, S., Fronzes, R. & Waksman, G. VirB2 and VirB5 proteins: specialized adhesins in bacterial type-  
605 IV secretion systems? *Trends in Microbiology* **16**, 409-413 (2008).  
606 <https://doi.org/https://doi.org/10.1016/j.tim.2008.07.001>

- 607 34 Bönig, T., Olbermann, P., Bats, S. H., Fischer, W. & Josenhans, C. Systematic site-directed mutagenesis  
608 of the *Helicobacter pylori* CagL protein of the Cag type IV secretion system identifies novel functional  
609 domains. *Sci Rep* **6**, 38101 (2016). <https://doi.org:10.1038/srep38101>
- 610 35 Pham, K. T. *et al.* CagI is an essential component of the *Helicobacter pylori* Cag type IV secretion system  
611 and forms a complex with CagL. *PLoS One* **7**, e35341 (2012).  
612 <https://doi.org:10.1371/journal.pone.0035341>
- 613 36 Khara, P., Song, L., Christie, P. J. & Hu, B. In Situ Visualization of the pKM101-Encoded Type IV Secretion  
614 System Reveals a Highly Symmetric ATPase Energy Center. *mBio* **12**, e0246521 (2021).  
615 <https://doi.org:10.1128/mBio.02465-21>
- 616 37 Liu, X., Khara, P., Baker, M. L., Christie, P. J. & Hu, B. Structure of a type IV secretion system core complex  
617 encoded by multi-drug resistance F plasmids. *Nature Communications* **13**, 379 (2022).  
618 <https://doi.org:10.1038/s41467-022-28058-5>
- 619 38 Kitao, T., Kubori, T. & Nagai, H. Recent advances in structural studies of the *Legionella pneumophila*  
620 Dot/Icm type IV secretion system. *Microbiol Immunol* **66**, 67-74 (2022). [https://doi.org:10.1111/1348-  
621 0421.12951](https://doi.org:10.1111/1348-0421.12951)
- 622 39 Gomez-Valero, L. *et al.* More than 18,000 effectors in the *Legionella* genus genome provide multiple,  
623 independent combinations for replication in human cells. *Proc Natl Acad Sci U S A* **116**, 2265-2273  
624 (2019). <https://doi.org:10.1073/pnas.1808016116>
- 625 40 Asrat, S., de Jesus, D. A., Hempstead, A. D., Ramabhadran, V. & Isberg, R. R. Bacterial pathogen  
626 manipulation of host membrane trafficking. *Annu Rev Cell Dev Biol* **30**, 79-109 (2014).  
627 <https://doi.org:10.1146/annurev-cellbio-100913-013439>
- 628 41 Durie, C. L. *et al.* Structural analysis of the *Legionella pneumophila* Dot/Icm type IV secretion system  
629 core complex. *Elife* **9** (2020). <https://doi.org:10.7554/eLife.59530>
- 630 **The first high-resolution structure of the *Legionella pneumophila* Dot/Icm T4SS, which plays a crucial**  
631 **role in niche establishment and the pathogenesis of Legionnaire's disease.**
- 632 42 Sheedlo, M. J. *et al.* Cryo-EM reveals new species-specific proteins and symmetry elements in the  
633 *Legionella pneumophila* Dot/Icm T4SS. *eLife* **10**, e70427 (2021). <https://doi.org:10.7554/eLife.70427>
- 634 43 Varga, M. G. *et al.* Pathogenic *Helicobacter pylori* strains translocate DNA and activate TLR9 via the  
635 cancer-associated cag type IV secretion system. *Oncogene* **35**, 6262-6269 (2016).  
636 <https://doi.org:10.1038/onc.2016.158>
- 637 44 Tegtmeyer, N., Neddermann, M., Asche, C. I. & Backert, S. Subversion of host kinases: a key network in  
638 cellular signaling hijacked by *Helicobacter pylori* CagA. *Mol Microbiol* **105**, 358-372 (2017).  
639 <https://doi.org:10.1111/mmi.13707>
- 640 45 Pfannkuch, L. *et al.* ADP heptose, a novel pathogen-associated molecular pattern identified in  
641 *Helicobacter pylori*. *Faseb j* **33**, 9087-9099 (2019). <https://doi.org:10.1096/fj.201802555R>
- 642 46 Cover, T. L., Lacy, D. B. & Ohi, M. D. The *Helicobacter pylori* Cag Type IV Secretion System. *Trends in*  
643 *Microbiology* **28**, 682-695 (2020). <https://doi.org:https://doi.org/10.1016/j.tim.2020.02.004>
- 644 47 Frick-Cheng, A. E. *et al.* Molecular and Structural Analysis of the *Helicobacter pylori* cag Type IV  
645 Secretion System Core Complex. *mBio* **7**, e02001-02015 (2016). [https://doi.org:10.1128/mBio.02001-  
646 15](https://doi.org:10.1128/mBio.02001-15)
- 647 48 Sheedlo, M. J. *et al.* Cryo-EM reveals species-specific components within the *Helicobacter pylori* Cag  
648 type IV secretion system core complex. *Elife* **9** (2020). <https://doi.org:10.7554/eLife.59495>
- 649 49 Hu, B., Khara, P. & Christie, P. J. Structural bases for F plasmid conjugation and F pilus biogenesis in  
650 *Escherichia coli*. *Proceedings of the National Academy of Sciences* **116**, 14222-14227 (2019).  
651 <https://doi.org:doi:10.1073/pnas.1904428116>
- 652 **The study presents the first in situ cryo-electron tomography visualization of the entire conjugative F**  
653 **T4SS, revealing four distinct conformational states of the machinery, and providing a step-by-step**

654 **mechanism of bacterial conjugation and pilus outgrowth, along with architectural representations of**  
655 **the machinery in each state.**

656 50 Ghosal, D., Chang, Y. W., Jeong, K. C., Vogel, J. P. & Jensen, G. J. In situ structure of the Legionella  
657 Dot/Icm type IV secretion system by electron cryotomography. *EMBO Rep* **18**, 726-732 (2017).  
658 <https://doi.org/10.15252/embr.201643598>

659 **The first cryo-electron tomography visualization of the Dot/Icm T4SS in *Legionella pneumophila***  
660 **revealing a common overall architecture shared across functionally diverse T4SSs.**

661 51 Chetrit, D., Hu, B., Christie, P. J., Roy, C. R. & Liu, J. A unique cytoplasmic ATPase complex defines the  
662 Legionella pneumophila type IV secretion channel. *Nature Microbiology* **3**, 678-686 (2018).  
663 <https://doi.org/10.1038/s41564-018-0165-z>

664 52 Park, D., Steiner, S., Shao, M., Roy, C. R. & Liu, J. Developmental Transitions Coordinate Assembly of the  
665 Coxiella burnetii Dot/Icm Type IV Secretion System. *Infect Immun* **90**, e0041022 (2022).  
666 <https://doi.org/10.1128/iai.00410-22>

667 53 Newton, H. J., McDonough, J. A. & Roy, C. R. Effector Protein Translocation by the Coxiella burnetii  
668 Dot/Icm Type IV Secretion System Requires Endocytic Maturation of the Pathogen-Occupied Vacuole.  
669 *PLOS ONE* **8**, e54566 (2013). <https://doi.org/10.1371/journal.pone.0054566>

670 54 Chang, Y. W., Shaffer, C. L., Rettberg, L. A., Ghosal, D. & Jensen, G. J. In Vivo Structures of the  
671 Helicobacter pylori cag Type IV Secretion System. *Cell Rep* **23**, 673-681 (2018).  
672 <https://doi.org/10.1016/j.celrep.2018.03.085>

673 55 Hu, B. *et al.* In Situ Molecular Architecture of the Helicobacter pylori Cag Type IV Secretion System.  
674 *mBio* **10** (2019). <https://doi.org/10.1128/mBio.00849-19>

675 56 Chung, J. M. *et al.* Structure of the Helicobacter pylori Cag type IV secretion system. *Elife* **8** (2019).  
676 <https://doi.org/10.7554/eLife.47644>

677 **The first high-resolution structure of the *Helicobacter pylori* Cag T4SS, which is required for *H. pylori***  
678 **infection of the human gastrointestinal tract.**

679 57 Tegtmeyer, N. *et al.* Toll-like Receptor 5 Activation by the CagY Repeat Domains of Helicobacter pylori.  
680 *Cell Rep* **32**, 108159 (2020). <https://doi.org/10.1016/j.celrep.2020.108159>

681 58 Audette, G. F., Manchak, J., Beatty, P., Klimke, W. A. & Frost, L. S. Entry exclusion in F-like plasmids  
682 requires intact TraG in the donor that recognizes its cognate TraS in the recipient. *Microbiology*  
683 (*Reading*) **153**, 442-451 (2007). <https://doi.org/10.1099/mic.0.2006/001917-0>

684 59 Marrero, J. & Waldor, M. K. Determinants of entry exclusion within Eex and TraG are cytoplasmic. *J*  
685 *Bacteriol* **189**, 6469-6473 (2007).

686 60 Gillespie, J. J. *et al.* An anomalous type IV secretion system in Rickettsia is evolutionarily conserved.  
687 *PLoS One* **4**, e4833 (2009). <https://doi.org/10.1371/journal.pone.0004833>

688 61 Gillespie, J. J. *et al.* Phylogenomics reveals a diverse Rickettsiales type IV secretion system. *Infect Immun*  
689 **78**, 1809-1823 (2010). <https://doi.org/10.1128/iai.01384-09>

690 62 Rancès, E., Voronin, D., Tran-Van, V. & Mavingui, P. Genetic and Functional Characterization of the Type  
691 IV Secretion System in *Wolbachia*. *Journal of Bacteriology* **190**, 5020-5030 (2008).  
692 <https://doi.org/doi:10.1128/JB.00377-08>

693 63 Nagai, H. & Roy, C. R. The DotA protein from Legionella pneumophila is secreted by a novel process that  
694 requires the Dot/Icm transporter. *Embo j* **20**, 5962-5970 (2001).  
695 <https://doi.org/10.1093/emboj/20.21.5962>

696 64 Skoog, E. C. *et al.* CagY-Dependent Regulation of Type IV Secretion in Helicobacter pylori Is Associated  
697 with Alterations in Integrin Binding. *MBio* **9** (2018). <https://doi.org/10.1128/mBio.00717-18>

698 65 Aras, R. A., Kang, J., Tschumi, A. I., Harasaki, Y. & Blaser, M. J. Extensive repetitive DNA facilitates  
699 prokaryotic genome plasticity. *Proc Natl Acad Sci U S A* **100**, 13579-13584 (2003).  
700 <https://doi.org/10.1073/pnas.1735481100>

- 701 66 Barrozo, R. M. *et al.* Functional Plasticity in the Type IV Secretion System of *Helicobacter pylori*. *PLOS*  
702 *Pathogens* **9**, e1003189 (2013). <https://doi.org/10.1371/journal.ppat.1003189>
- 703 67 Llosa, M. & Alkorta, I. in *Type IV Secretion in Gram-Negative and Gram-Positive Bacteria* (eds Steffen  
704 Backert & Elisabeth Grohmann) 143-168 (Springer International Publishing, 2017).
- 705 68 Gomis-Rüth, F. X. *et al.* The bacterial conjugation protein TrwB resembles ring helicases and F1-ATPase.  
706 *Nature* **409**, 637-641 (2001). <https://doi.org/10.1038/35054586>
- 707 69 Whitaker, N. *et al.* The All-Alpha Domains of Coupling Proteins from the *Agrobacterium tumefaciens*  
708 VirB/VirD4 and *Enterococcus faecalis* pCF10-Encoded Type IV Secretion Systems Confer Specificity to  
709 Binding of Cognate DNA Substrates. *Journal of Bacteriology* **197**, 2335-2349 (2015).  
710 <https://doi.org/doi:10.1128/JB.00189-15>
- 711 70 Oka, G. U. *et al.* Structural basis for effector recognition by an antibacterial type IV secretion system.  
712 *Proceedings of the National Academy of Sciences* **119**, e2112529119 (2022).  
713 <https://doi.org/doi:10.1073/pnas.2112529119>
- 714 71 Atmakuri, K., Cascales, E. & Christie, P. J. Energetic components VirD4, VirB11 and VirB4 mediate early  
715 DNA transfer reactions required for bacterial type IV secretion. *Mol Microbiol* **54**, 1199-1211 (2004).  
716 <https://doi.org/10.1111/j.1365-2958.2004.04345.x>
- 717 72 Ripoll-Rozada, J., Zunzunegui, S., de la Cruz, F., Arechaga, I. & Cabezón, E. Functional interactions of  
718 VirB11 traffic ATPases with VirB4 and VirD4 molecular motors in type IV secretion systems. *J Bacteriol*  
719 **195**, 4195-4201 (2013). <https://doi.org/10.1128/JB.00437-13>
- 720 73 Savvides, S. N. *et al.* VirB11 ATPases are dynamic hexameric assemblies: new insights into bacterial type  
721 IV secretion. *EMBO J.* **22**, 1969-1980 (2003).
- 722 74 Hare, S., Bayliss, R., Baron, C. & Waksman, G. A Large Domain Swap in the VirB11 ATPase of *Brucella*  
723 *suis* Leaves the Hexameric Assembly Intact. *Journal of molecular biology* **360**, 56-66 (2006).  
724 <https://doi.org/https://doi.org/10.1016/j.jmb.2006.04.060>
- 725 75 Park, D., Chetrit, D., Hu, B., Roy, C. R. & Liu, J. Analysis of Dot/Icm Type IVB Secretion System  
726 Subassemblies by Cryoelectron Tomography Reveals Conformational Changes Induced by DotB Binding.  
727 *mBio* **11**, e03328-03319 (2020). <https://doi.org/doi:10.1128/mBio.03328-19>
- 728 76 Sagulenko, E., Sagulenko, V., Chen, J. & Christie, P. J. Role of *Agrobacterium* VirB11 ATPase in T-pilus  
729 assembly and substrate selection. *Journal of Bacteriology* **183**, 5813-5825 (2001).  
730 <https://doi.org/10.1128/JB.183.20.5813-5825.2001>
- 731 77 Hilleringmann, M. *et al.* Inhibitors of *Helicobacter pylori* ATPase Cag $\alpha$  block CagA transport and cag  
732 virulence. *Microbiology* **152**, 2919-2930 (2006). <https://doi.org/https://doi.org/10.1099/mic.0.28984-0>
- 733 78 Nagai, H. *et al.* A C-terminal translocation signal required for Dot/Icm-dependent delivery of the  
734 *Legionella* RalF protein to host cells. *Proceedings of the National Academy of Sciences* **102**, 826-831  
735 (2005).
- 736 79 Cambronne, E. D. & Roy, C. R. The *Legionella pneumophila* IcmSW Complex Interacts with Multiple  
737 Dot/Icm Effectors to Facilitate Type IV Translocation. *PLOS Pathogens* **3**, e188 (2007).  
738 <https://doi.org/10.1371/journal.ppat.0030188>
- 739 80 Kim, H. *et al.* Structural basis for effector protein recognition by the Dot/Icm Type IVB coupling protein  
740 complex. *Nature communications* **11**, 1-11 (2020).
- 741 81 Jeong, K. C., Sutherland, M. C. & Vogel, J. P. Novel export control of a *Legionella* Dot/Icm substrate is  
742 mediated by dual, independent signal sequences. *Mol Microbiol* **96**, 175-188 (2015).  
743 <https://doi.org/10.1111/mmi.12928>
- 744 82 Meir, A., Chetrit, D., Liu, L., Roy, C. R. & Waksman, G. *Legionella* DotM structure reveals a role in effector  
745 recruiting to the Type 4B secretion system. *Nature Communications* **9**, 507 (2018).  
746 <https://doi.org/10.1038/s41467-017-02578-x>
- 747 **The paper presents the crystallographic structure of DotM, revealing a novel mechanism of effector**  
748 **recognition by the Dot/Icm T4SS in *Legionella pneumophila*.**

- 749 83 Mace, K. *et al.* Proteins DotY and DotZ modulate the dynamics and localization of the type IVB coupling  
750 complex of Legionella pneumophila. *Mol Microbiol* **117**, 307-319 (2022).  
751 <https://doi.org:10.1111/mmi.14847>
- 752 84 Meir, A., Macé, K., Vegunta, Y., Williams, S. M. & Waksman, G. Substrate recruitment mechanism by  
753 gram-negative type III, IV, and VI bacterial injectisomes. *Trends Microbiol* (2023).  
754 <https://doi.org:10.1016/j.tim.2023.03.005>
- 755 85 Kwak, M. J. *et al.* Architecture of the type IV coupling protein complex of Legionella pneumophila. *Nat*  
756 *Microbiol* **2**, 17114 (2017). <https://doi.org:10.1038/nmicrobiol.2017.114>
- 757 86 Meir, A. *et al.* Mechanism of effector capture and delivery by the type IV secretion system from  
758 Legionella pneumophila. *Nature Communications* **11**, 2864 (2020). [https://doi.org:10.1038/s41467-](https://doi.org:10.1038/s41467-020-16681-z)  
759 [020-16681-z](https://doi.org:10.1038/s41467-020-16681-z)
- 760 87 Vincent, C. D., Friedman, J. R., Jeong, K. C., Sutherland, M. C. & Vogel, J. P. Identification of the DotL  
761 coupling protein subcomplex of the Legionella Dot/Icm type IV secretion system. *Molecular*  
762 *microbiology* **85**, 378-391 (2012). <https://doi.org:10.1111/j.1365-2958.2012.08118.x>
- 763 88 Xu, J. *et al.* Structural insights into the roles of the IcmS–IcmW complex in the type IVb secretion system  
764 of Legionella pneumophila. *Proceedings of the National Academy of Sciences* **114**, 13543-13548 (2017).
- 765 89 Pattis, I., Weiss, E., Laugks, R., Haas, R. & Fischer, W. The *Helicobacter pylori* CagF protein is a type IV  
766 secretion chaperone-like molecule that binds close to the C-terminal secretion signal of the CagA  
767 effector protein. *Microbiology* **153**, 2896-2909 (2007). <https://doi.org:10.1099/mic.0.2007/007385-0>
- 768 90 Wu, X. *et al.* Mechanism of regulation of the *Helicobacter pylori* Cagβ ATPase by CagZ. *Nature*  
769 *Communications* **14**, 479 (2023). <https://doi.org:10.1038/s41467-023-36218-4>
- 770 91 de la Cruz, F., Frost, L. S., Meyer, R. J. & Zechner, E. L. Conjugative DNA metabolism in Gram-negative  
771 bacteria. *FEMS microbiology reviews* **34**, 18-40 (2010). [https://doi.org:10.1111/j.1574-](https://doi.org:10.1111/j.1574-6976.2009.00195.x)  
772 [6976.2009.00195.x](https://doi.org:10.1111/j.1574-6976.2009.00195.x)
- 773 92 Ilangovan, A. *et al.* Cryo-EM Structure of a Relaxase Reveals the Molecular Basis of DNA Unwinding  
774 during Bacterial Conjugation. *Cell* **169**, 708-721.e712 (2017).  
775 <https://doi.org:https://doi.org/10.1016/j.cell.2017.04.010>
- 776 **The study reveals the first structure of the relaxase protein, the core component of the relaxosome**  
777 **complex involved in DNA processing prior to conjugation, showing that two distinct activities of the**  
778 **relaxase, the trans-esterase activity required for DNA nicking, and the helicase activity essential for**  
779 **DNA unwinding, are simultaneously performed by two distinct structural conformers.**
- 780 93 Datta, S., Larkin, C. & Schildbach, J. F. Structural insights into single-stranded DNA binding and cleavage  
781 by F factor TraI. *Structure* **11**, 1369-1379 (2003).
- 782 94 Rice, P. A., Yang, S., Mizuuchi, K. & Nash, H. A. Crystal structure of an IHF-DNA complex: a protein-  
783 induced DNA U-turn. *Cell* **87**, 1295-1306 (1996).
- 784 95 Luo, Y., Gao, Q. & Deonier, R. C. Mutational and physical analysis of F plasmid *traY* protein binding to  
785 *oriT*. *Mol Microbiol* **11**, 459-469 (1994).
- 786 96 Lu, J. *et al.* Structural basis of specific TraD–TraM recognition during F plasmid-mediated bacterial  
787 conjugation. *Molecular Microbiology* **70**, 89-99 (2008). [https://doi.org:https://doi.org/10.1111/j.1365-](https://doi.org:https://doi.org/10.1111/j.1365-2958.2008.06391.x)  
788 [2958.2008.06391.x](https://doi.org:https://doi.org/10.1111/j.1365-2958.2008.06391.x)
- 789 97 Beranek, A. *et al.* Thirty-Eight C-Terminal Amino Acids of the Coupling Protein TraD of the F-Like  
790 Conjugative Resistance Plasmid R1 Are Required and Sufficient To Confer Binding to the Substrate  
791 Selector Protein TraM. *Journal of Bacteriology* **186**, 6999-7006 (2004).  
792 <https://doi.org:doi:10.1128/JB.186.20.6999-7006.2004>
- 793 98 Wong, J. J., Lu, J., Edwards, R. A., Frost, L. S. & Glover, J. M. Structural basis of cooperative DNA  
794 recognition by the plasmid conjugation factor, TraM. *Nucleic acids research* **39**, 6775-6788 (2011).

- 795 99 Rêgo, A. T., Chandran, V. & Waksman, G. Two-step and one-step secretion mechanisms in Gram-  
796 negative bacteria: contrasting the type IV secretion system and the chaperone-usher pathway of pilus  
797 biogenesis. *Biochem J* **425**, 475-488 (2010). <https://doi.org:10.1042/bj20091518>
- 798 100 Prevost, M. S. & Waksman, G. X-ray crystal structures of the type IVb secretion system DotB ATPases.  
799 *Protein Sci* **27**, 1464-1475 (2018). <https://doi.org:10.1002/pro.3439>
- 800 101 Jakubowski, S. J., Cascales, E., Krishnamoorthy, V. & Christie, P. J. *Agrobacterium tumefaciens* VirB9, an  
801 outer-membrane-associated component of a type IV secretion system, regulates substrate selection  
802 and T-pilus biogenesis. *J Bacteriol* **187**, 3486-3495 (2005).
- 803 102 Redzej, A. *et al.* Structure of a VirD4 coupling protein bound to a VirB type IV secretion machinery. *The*  
804 *EMBO Journal* **36**, 3080-3095 (2017). <https://doi.org:https://doi.org/10.15252/embj.201796629>
- 805 103 Burns, D. L. Secretion of Pertussis Toxin from *Bordetella pertussis*. *Toxins* **13**, 574 (2021).
- 806 104 Dehio, C. & Tsolis, R. M. Type IV Effector Secretion and Subversion of Host Functions by *Bartonella* and  
807 *Brucella* Species. *Curr Top Microbiol Immunol* **413**, 269-295 (2017). [https://doi.org:10.1007/978-3-319-75241-9\\_11](https://doi.org:10.1007/978-3-319-75241-9_11)
- 808
- 809 105 Costa, T. R. D. *et al.* Structure of the Bacterial Sex F Pilus Reveals an Assembly of a Stoichiometric  
810 Protein-Phospholipid Complex. *Cell* **166**, 1436-1444 e1410 (2016).  
811 <https://doi.org:10.1016/j.cell.2016.08.025>
- 812 **The paper presents the structure of the conjugative F pilus, uncovering the incorporation of**  
813 **phospholipid molecules within the pilus filament's molecular architecture, establishing the basis for**  
814 **structural characterization of conjugative pili and leading to a surge in available architectures of other**  
815 **conjugative pili with their respective phospholipid types.**
- 816 106 Zheng, W. *et al.* Cryoelectron-Microscopic Structure of the pKpQL Conjugative Pili from Carbapenem-  
817 Resistant *Klebsiella pneumoniae*. *Structure* **28**, 1321-1328.e1322 (2020).  
818 <https://doi.org:10.1016/j.str.2020.08.010>
- 819 107 Kreida, S. *et al.* Cryo-EM structure of the *Agrobacterium tumefaciens* T4SS-associated T-pilus reveals  
820 stoichiometric protein-phospholipid assembly. *Structure* (2023).  
821 <https://doi.org:10.1016/j.str.2023.02.005>
- 822 108 Amro, J. *et al.* Cryo-EM structure of the *Agrobacterium tumefaciens* T-pilus reveals the importance of  
823 positive charges in the lumen. *Structure* **31**, 375-384 (2023). <https://doi.org:10.1016/j.str.2022.11.007>
- 824 109 Beltran, L. C. *et al.* Archaeal DNA-import apparatus is homologous to bacterial conjugation machinery.  
825 *Nature Communications* **14**, 666 (2023). <https://doi.org:10.1038/s41467-023-36349-8>
- 826 110 Patkowski, J. B. *et al.* The F-pilus biomechanical adaptability accelerates conjugative dissemination of  
827 antimicrobial resistance and biofilm formation. *Nature Communications* **14**, 1879 (2023).  
828 <https://doi.org:10.1038/s41467-023-37600-y>
- 829 111 Rozwandowicz, M. *et al.* Plasmids carrying antimicrobial resistance genes in Enterobacteriaceae. *J*  
830 *Antimicrob Chemother* **73**, 1121-1137 (2018). <https://doi.org:10.1093/jac/dkx488>
- 831 112 Bradley, D. E. Morphological and serological relationships of conjugative pili. *Plasmid* **4**, 155-169 (1980).
- 832 113 Paschos, A. *et al.* An in vivo high-throughput screening approach targeting the type IV secretion system  
833 component VirB8 identified inhibitors of *Brucella abortus* 2308 proliferation. *Infection and immunity*  
834 **79**, 1033-1043 (2011). <https://doi.org:10.1128/IAI.00993-10>
- 835 114 Shaffer, C. L. *et al.* Peptidomimetic Small Molecules Disrupt Type IV Secretion System Activity in Diverse  
836 Bacterial Pathogens. *MBio* **7**, e00221-00216 (2016). <https://doi.org:10.1128/mBio.00221-16>
- 837 115 Ripoll-Rozada, J. *et al.* Type IV traffic ATPase TrwD as molecular target to inhibit bacterial conjugation.  
838 *Mol Microbiol* **100**, 912-921 (2016). <https://doi.org:10.1111/mmi.13359>
- 839 116 Casu, B., Arya, T., Bessette, B. & Baron, C. Fragment-based screening identifies novel targets for  
840 inhibitors of conjugative transfer of antimicrobial resistance by plasmid pKM101. *Scientific Reports* **7**,  
841 14907 (2017). <https://doi.org:10.1038/s41598-017-14953-1>

- 842 117 Getino, M. & de la Cruz, F. Natural and Artificial Strategies To Control the Conjugative Transmission of  
843 Plasmids. *Microbiol Spectr* **6** (2018). <https://doi.org:10.1128/microbiolspec.MTBP-0015-2016>
- 844 118 Garcia-Cazorla, Y. *et al.* Conjugation inhibitors compete with palmitic acid for binding to the conjugative  
845 traffic ATPase TrwD, providing a mechanism to inhibit bacterial conjugation. *J Biol Chem* **293**, 16923-  
846 16930 (2018). <https://doi.org:10.1074/jbc.RA118.004716>
- 847 119 Arya, T. *et al.* Fragment-based screening identifies inhibitors of ATPase activity and of hexamer  
848 formation of Cagalpha from the Helicobacter pylori type IV secretion system. *Sci Rep* **9**, 6474 (2019).  
849 <https://doi.org:10.1038/s41598-019-42876-6>
- 850 120 Alvarez-Rodríguez, I. *et al.* Type IV Coupling Proteins as Potential Targets to Control the Dissemination  
851 of Antibiotic Resistance. *Front Mol Biosci* **7**, 201 (2020). <https://doi.org:10.3389/fmolb.2020.00201>
- 852 121 Brown, P. J. B., Chang, J. H. & Fuqua, C. Agrobacterium tumefaciens: a Transformative Agent for  
853 Fundamental Insights into Host-Microbe Interactions, Genome Biology, Chemical Signaling, and Cell  
854 Biology. *J Bacteriol*, e0000523 (2023). <https://doi.org:10.1128/jb.00005-23>
- 855 122 Hamilton, T. A. *et al.* Efficient inter-species conjugative transfer of a CRISPR nuclease for targeted  
856 bacterial killing. *Nature Communications* **10**, 4544 (2019). <https://doi.org:10.1038/s41467-019-12448-3>  
857
- 858 123 Vrancianu, C. O., Popa, L. I., Bleotu, C. & Chifiriuc, M. C. Targeting Plasmids to Limit Acquisition and  
859 Transmission of Antimicrobial Resistance. *Front Microbiol* **11**, 761 (2020).  
860 <https://doi.org:10.3389/fmicb.2020.00761>
- 861 124 Reuter, A. *et al.* Targeted-antibacterial-plasmids (TAPs) combining conjugation and CRISPR/Cas systems  
862 achieve strain-specific antibacterial activity. *Nucleic Acids Res* **49**, 3584-3598 (2021).  
863 <https://doi.org:10.1093/nar/gkab126>
- 864 125 Bier, E. & Nizet, V. Driving to Safety: CRISPR-Based Genetic Approaches to Reducing Antibiotic  
865 Resistance. *Trends Genet* **37**, 745-757 (2021). <https://doi.org:10.1016/j.tig.2021.02.007>
- 866 126 Robledo, M. *et al.* Targeted bacterial conjugation mediated by synthetic cell-to-cell adhesions. *Nucleic  
867 Acids Res* **50**, 12938-12950 (2022). <https://doi.org:10.1093/nar/gkac1164>

868

869

870 **Figure 1. The functional versatility of type IV secretion systems.**

871 Various pathogenic bacteria and symbionts deploy type IV secretion systems (T4SSs) to deliver effector proteins,  
872 DNA–protein complexes or other macromolecules into eukaryotic or protozoan host cells. **a** | The T4SSs  
873 establishes contact dependent interkingdom interactions by injecting effectors directly into eukaryotic cells to  
874 promote bacterial intracellular survival and symbiosis. **b** | Many bacterial species and a few Archaea deploy a  
875 contact-dependent T4SSs for the delivery of DNA and toxins to other bacteria or Archaea. Various species in the  
876 *Xanthomonadales* instead deploy T4SSs for the contact-dependent delivery of protein toxins to kill other  
877 bacteria for niche establishment. **c** | Some bacteria can deploy T4SSs for the contact-independent uptake or  
878 release of DNA.

879

880 **Figure 2. Structure of minimal type IV secretion system and pilus biogenesis mechanism model.**

881 **a** | Global organisation to atomic details of the minimised R388-encoded type IV secretion system (T4SS). The  
882 entire cryo-electron microscopy (cryo-EM) structure of the R388 T4SS is shown with half-left in cryo-EM density  
883 colored by sub-complexes (Electron Microscopy Data Bank (EMDB) entry 12707, EMDB 12708, EMDB 12709,  
884 EMDB 13767 and EMDB 12933) and half-right in ribbon and surface semi-transparent representation colored by



885 proteins (Protein Data Bank (PDB) identifier 7O3J, PDB ID 7O3T, PDB ID 7O3V, PDB ID 7Q1V and PDB ID 7OIU).  
886 At top-left corner, the cryo-ET of pKM101 T4SS density (EMDB 24098 and 24100) colored by sub-complexes is  
887 displayed to show that the structure of purified R388 T4SS is similar to the *in situ* T4SS structure. For each sub-  
888 complex, structure details, symmetry and membrane localisation are indicated. Black dashed lines demarcate  
889 the boundaries of the outer membrane and inner membrane. **b** | Model of pilus biogenesis mechanism. The  
890 T4SS is schematically represented in slice-view and colored by protein. Four states are shown: T4SS in similar  
891 state as observed by cryo-EM and shown in part a (1). The pilus biogenesis state with VirB11 bound at the  
892 bottom of VirB4; VirB2 is extracted from the inner membrane and recruited to VirB6 through the coordinated  
893 actions of the VirB4–VirB11 ATPases (2). As layers of VirB2 are recruited, the pilus grows from the VirB6  
894 assembly sites and VirB5 remains at the pilus tip (3). As the pilus grows, the O-layer of the OMCC opens up and  
895 the pilus with VirB5 at the tip extends into the extracellular milieu to establish contact with potential recipient  
896 cells (4). Part a is adapted with permission from Ref 14.

897

898 **Figure 3. Structural organisation of expanded type IV secretion system.**

899 **a** | Three expanded type IV secretion system (T4SS) outer membrane core complex (OMCC) structures are  
900 shown. The OMCC of the F-plasmid (Protein Data Bank (PDB) identifier 7OKN and PDB ID 7OKO), *Legionella*  
901 *pneumophila* (PDB ID 7MUS) and *Helicobacter pylori* (PDB ID 6X6S and 6X6J) are shown in surface representation  
902 and colored in dark red, blue and green for the VirB7-, VirB9- and VirB10-like proteins, respectively, and in grey  
903 for other components. Notably, *L. pneumophila* and *H. pylori* OMCCs contain an outer membrane cap (OMC)  
904 and a periplasmic ring (PR). **b** | Cryo-tomography maps of the F-plasmid with and without pilus. The maps  
905 (Electron Microscopy Data Bank (EMDB) entry 9344 and 9347) are colored by subcomplexes (that is; green for  
906 the OMCC, red for the Stalk, yellow for the Arches, blue for the inner membrane complex (IMC) and grey for the  
907 pilus. The junction of the pilus and Stalk is not well defined. **c** | Cryo-electron microscopy (cryo-ET) map of the  
908 *L. pneumophila* T4SS (EMDB entry 7611 and 7612) colored as in b, in front and slice view. **d** | Cryo-ET of the *H.*  
909 *pylori* T4SS (EMDB entry 0634 and 0635) colored as in b, in front and slice view.

910

911 **Figure 4. Examples of type IV secretion system subunit adaptations for functional diversification.**

912 The R388-encoded type IV secretion system T4SS is shown at left for reference. VirB5 subunits are deployed for  
913 binding of target-cell receptors; these subunits can localize at the tips of conjugative pili or on the bacterial cell  
914 surface. Some bacteria encode several copies of VirB2 or VirB5 subunits whose variable sequences are  
915 postulated to bind different target-cell receptors or contribute to evasion of the host immune system. Extended  
916 VirB6 carry large hydrophilic domains, several of which have been shown or are implicated in localizing at the  
917 cell surface to promote adhesion or immunomodulation, or blocking redundant plasmid transfer. F systems  
918 elaborate F pili that dynamically extend and retract to establish contacts with potential recipient cells at a  
919 distance. F systems also code for TraN subunits, whose extracellular domains interact with outer membrane  
920 proteins (OMPs) on recipient cells to promote F plasmid transfer and specify plasmid host range. Several T4SSs  
921 possess variant forms of the VirB7–VirB9–VirB10 core complex subunits, as exemplified for CagY in the *H. pylori*  
922 Cag system. The *H. pylori* system elaborates a conjugative pilus, which is decorated by other Cag subunits as well

923 as the CagA secretion substrate. Various T4SSs functionally interact with other surface adhesins, such as  
924 pKM101-encoded Pep or *H. pylori* OMPs, to promote target-cell binding.

925

926 **Figure 5. Structure of VirD4- and VirB11-like ATPases.**

927 **a** | Side and top view of two VirD4-like ATPase structures: TrwB from R388 plasmid (Protein Data Bank (PDB)  
928 identifier (ID) 1GKI) and Cag $\beta$  from *H. pylori* (PDB ID 8DOL). Structures are shown in ribbon representation and  
929 colored by monomer. **b** | Side and top view of two VirB11-like ATPase structures; DotB from *L. pneumophila*  
930 (PDB ID 6GEF) and Cag $\alpha$  from *H. pylori* (PDB ID 1NLZ). Structures are shown in ribbon representation and colored  
931 by monomer. **c** | Organisation and structure of type 4 coupling complex (T4CC) from *L. pneumophila*. The  
932 monomeric cryo- electron microscopy (cryo-EM) structure of the T4CC (PDB ID 6SZ9) is shown in surface  
933 representation and colored by protein: VirD4-like DotL in red), DotM in cyan, DotN in blue, DotZ in yellow, DotY  
934 in green, IcmS in pink and IcmW in purple. The module made up of the extreme C-terminus of (DotL<sub>C-ter</sub>) and  
935 IcmSW is flexible, and its motion area is represented in mesh. Crystal structure of the DotL<sub>C-ter</sub>–IcmSW module  
936 in presence of LvgA adaptor (orange) and VpdB substrate (black) is shown (PDB ID 7BWK). On the right, a model  
937 of the hexameric T4CC structure is shown in front and top views using the same color coding as in part c.

938

939 **Figure 6. Models for substrates recruitment and transport through the type IV secretion system.**

940 **a** | Conjugative type IV secretion system (T4SS) recruitment and secretion mechanism model. Silhouette of F-  
941 plasmid T4SS is shown in green. First, the DNA is processed by a relaxosomal complex made of TraM (green),  
942 TraY (turquoise), IHF (purple) and TraI (light brown). The relaxosome is recruited by TraD<sub>VirD4</sub> ATPase, which  
943 energizes the secretion of the TraI–ssDNA through the T4SS apparatus into the host. The relative position of  
944 TraD<sub>VirD4</sub> and the global organisation of the inner membrane complex (IMC) during DNA secretion is unknown. **b**  
945 | T4SS effector recruitment and secretion mechanism model. Silhouette of *L. pneumophila* Dot/Icm T4SS is  
946 shown in blue. The type IV coupling complex (T4CC) acts as a effector recruitment platform and is schematically  
947 represented and positioned beside the complex formed by the hexameric dimers of DotO and DotB, although  
948 its precise localisation is unknown. Effector proteins are captured by the T4CC at different binding sites and  
949 DotL<sub>VirD4</sub> energizes substrate translocation via one of two possible routes across the inner membrane. Route 1:  
950 The T4CC feeds substrates into the DotO–DotB energy centre at the base of the T4SS channel for transit in one-  
951 step across the entire cell envelope. Route 2: the T4CC feeds substrates into the lumen of the DotL hexamer for  
952 delivery across the inner membrane. In a second translocation step, substrates are recruited from the periplasm  
953 by the T4SS channel for passage to the cell surface and into target cells. Part b is adapted with permission from  
954 Ref. 28.

955

956 **Figure 7. Structure comparison between minimal, expanded and archaea pilus.**

957 **a** | Side view of all known pilus structures. Pilus structures (Protein Data Bank (PDB) identifier (ID) 8EXH  
958 *Agrobacterium tumefaciens* T-pilus, PDB ID 8CW4 *Escherichia coli* N-pilus; PDB ID 5LER *E. coli* F-pilus; PDB ID  
959 5LEG *Salmonella typhimurium* pED208; PDB ID 7JSV *Klebsiella pneumoniae* pKpQIL; PDB ID 8DFU *Aeropyrum*  
960 *pernix* CedA1 and PDB ID 8DFT *Pyrobaculum calidifontis* TedC) are in surface representation with one strand

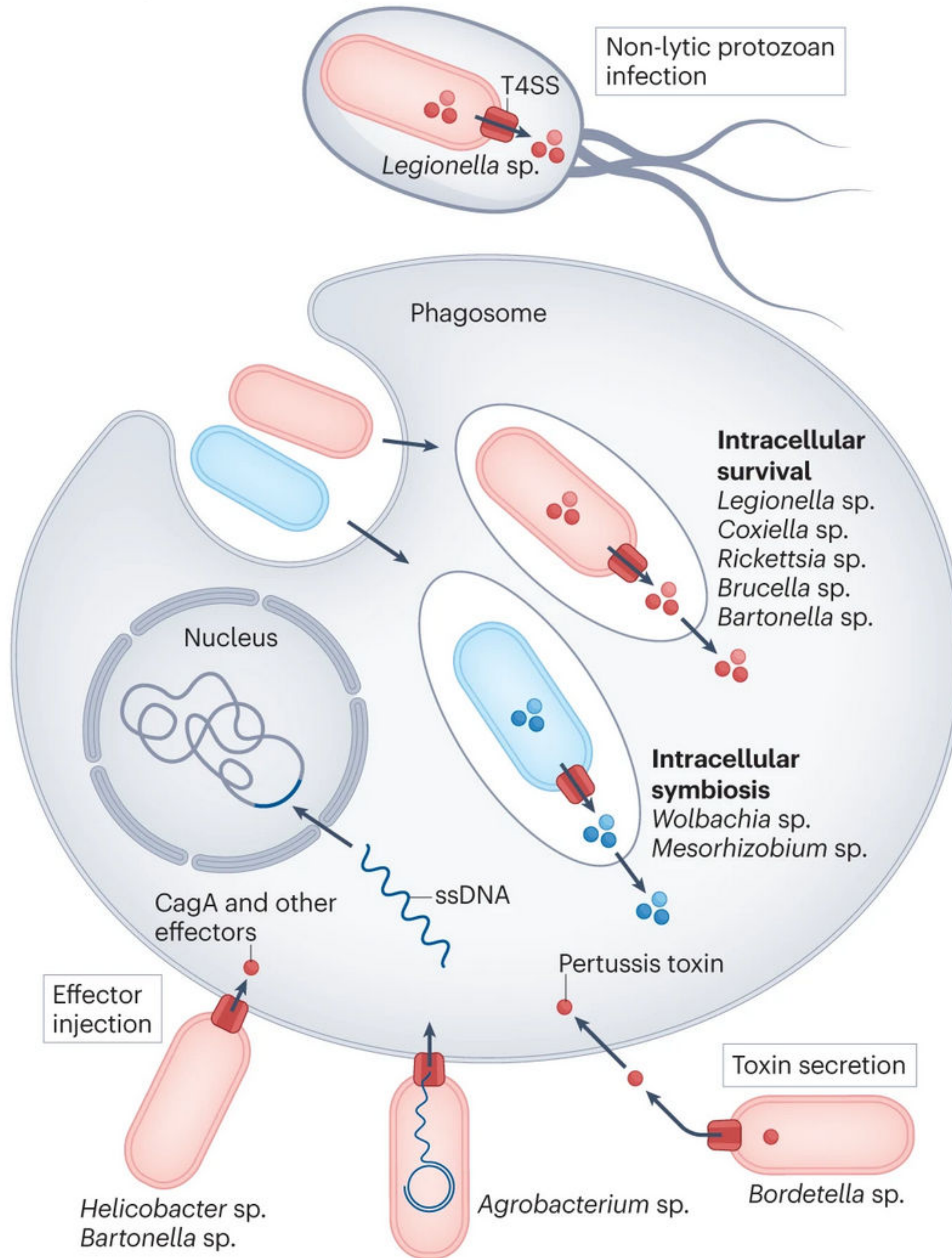
961 colored in grey. **b** | Top view of pilus structures. Diameter and lumen sizes are indicated. **c** | For each pilus, one  
962 monomer of VirB2 with its lipid is shown in ribbon representation. Arrows in the minimised type IV secretion  
963 systems (T4SSs) highlight the presence of a 'kink', which is characteristic of this group. Parts a and b adapted  
964 with permission from Ref. 109.

# Fig. 1: The functional versatility of type IV secretion systems.

From: [Structural and functional diversity of type IV secretion systems](#)

**a**

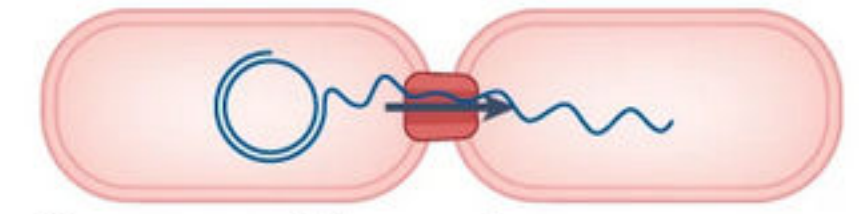
## Contact-dependent interkingdom



**b**

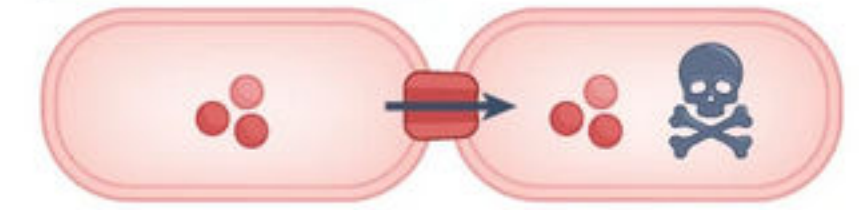
## Contact-dependent interbacterial

### Conjugation



Gram-positive and Gram-negative bacteria

### Toxin delivery

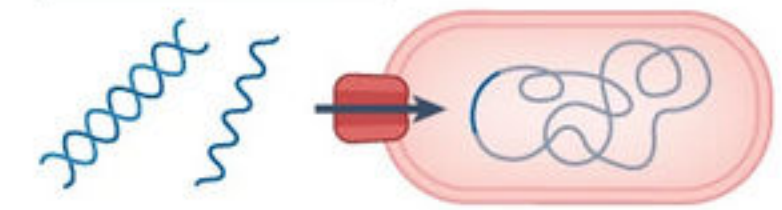


*Xanthomonadales*

**c**

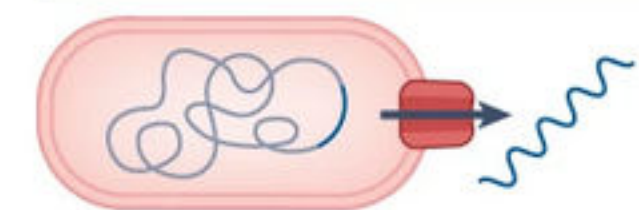
## Contact-independent DNA uptake or release

### DNA uptake



*Helicobacter pylori*

### DNA release and biofilm formation

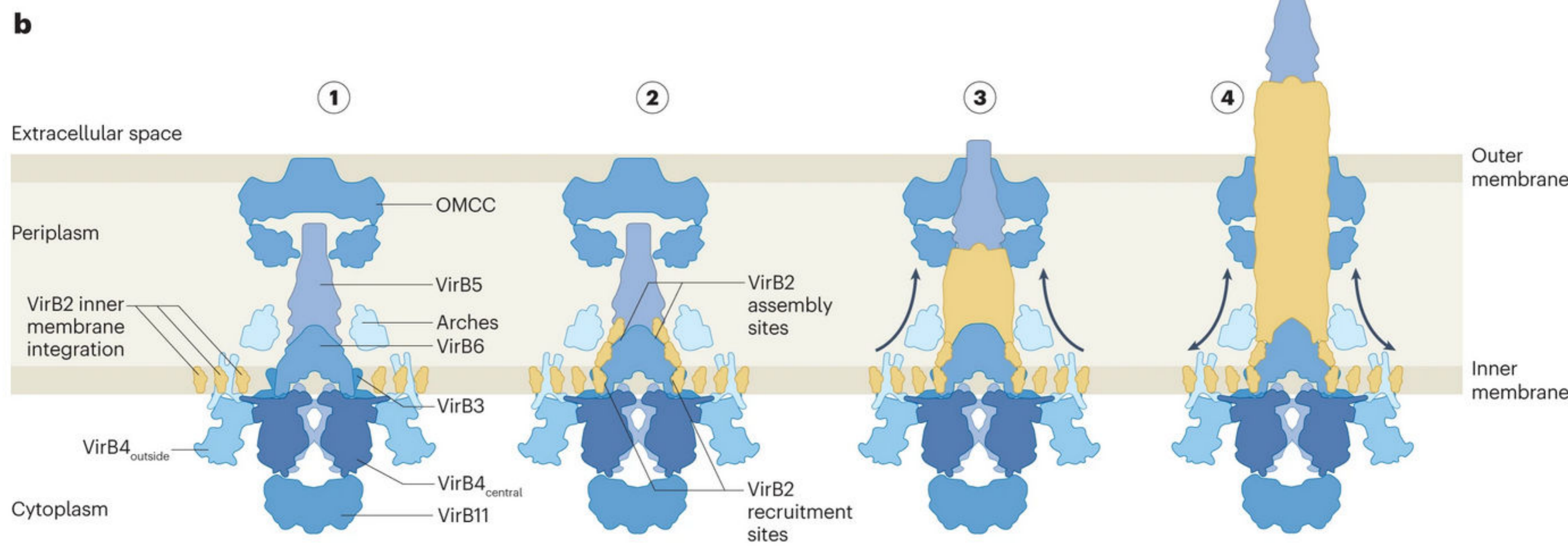
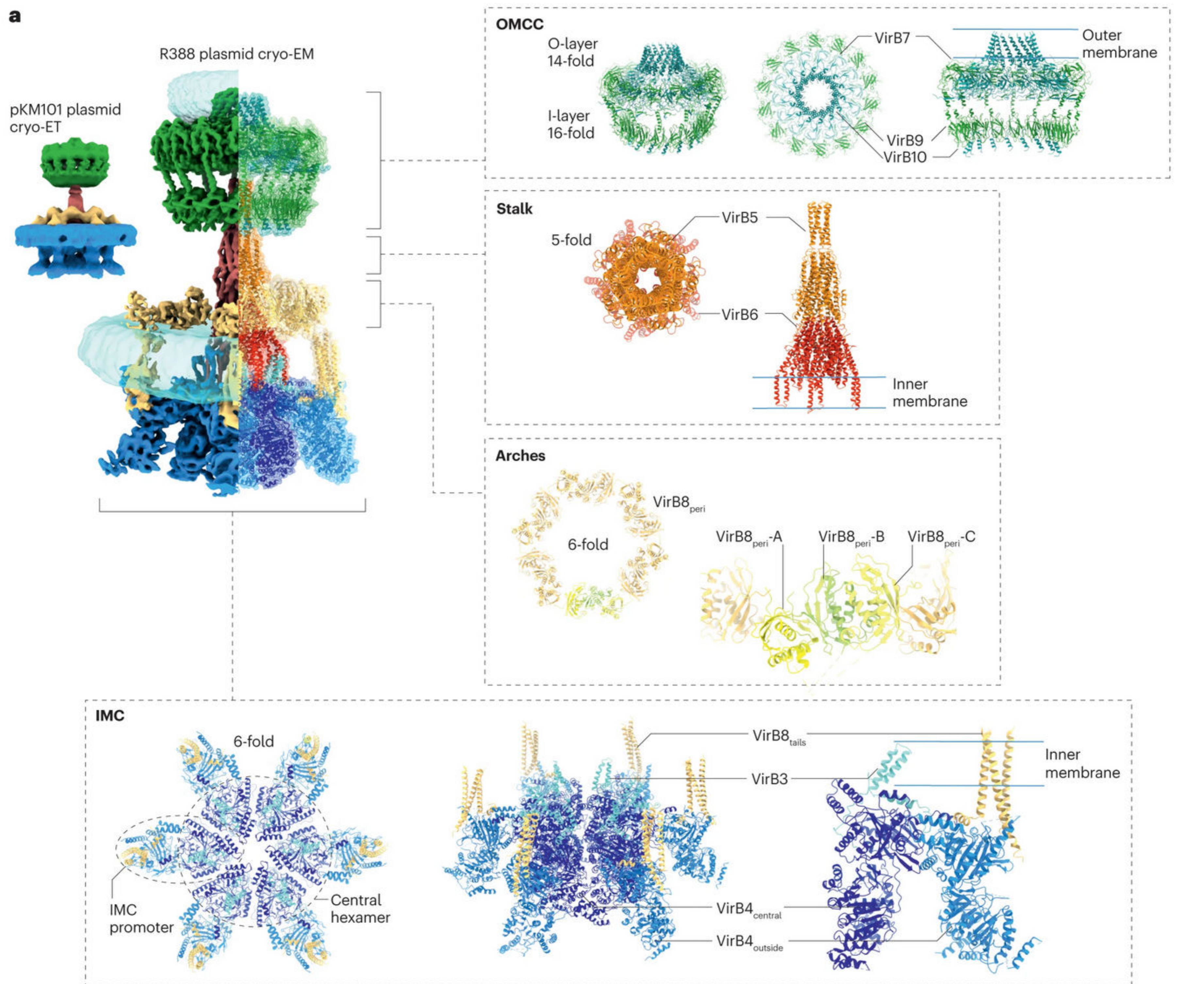


*Neisseria gonorrhoeae*

Various pathogenic bacteria and symbionts deploy type IV secretion systems (T4SSs) to deliver effector proteins, DNA-protein complexes or other macromolecules into eukaryotic or protozoan host cells. **a**, The T4SS establishes contact-dependent interkingdom interactions by injecting effectors directly into eukaryotic cells to promote bacterial intracellular survival and symbiosis. **b**, Many bacterial species and a few Archaea deploy a contact-dependent T4SS for the delivery of DNA and toxins to other bacteria or Archaea. Various species in the *Xanthomonadales* instead deploy T4SSs for the contact-dependent delivery of protein toxins to kill other bacteria for niche establishment. **c**, Some bacteria can deploy T4SSs for the contact-independent uptake or release of DNA. ssDNA, single-stranded DNA.

## Fig. 2: Structure of minimal type IV secretion system and pilus biogenesis mechanism model.

From: [Structural and functional diversity of type IV secretion systems](#)

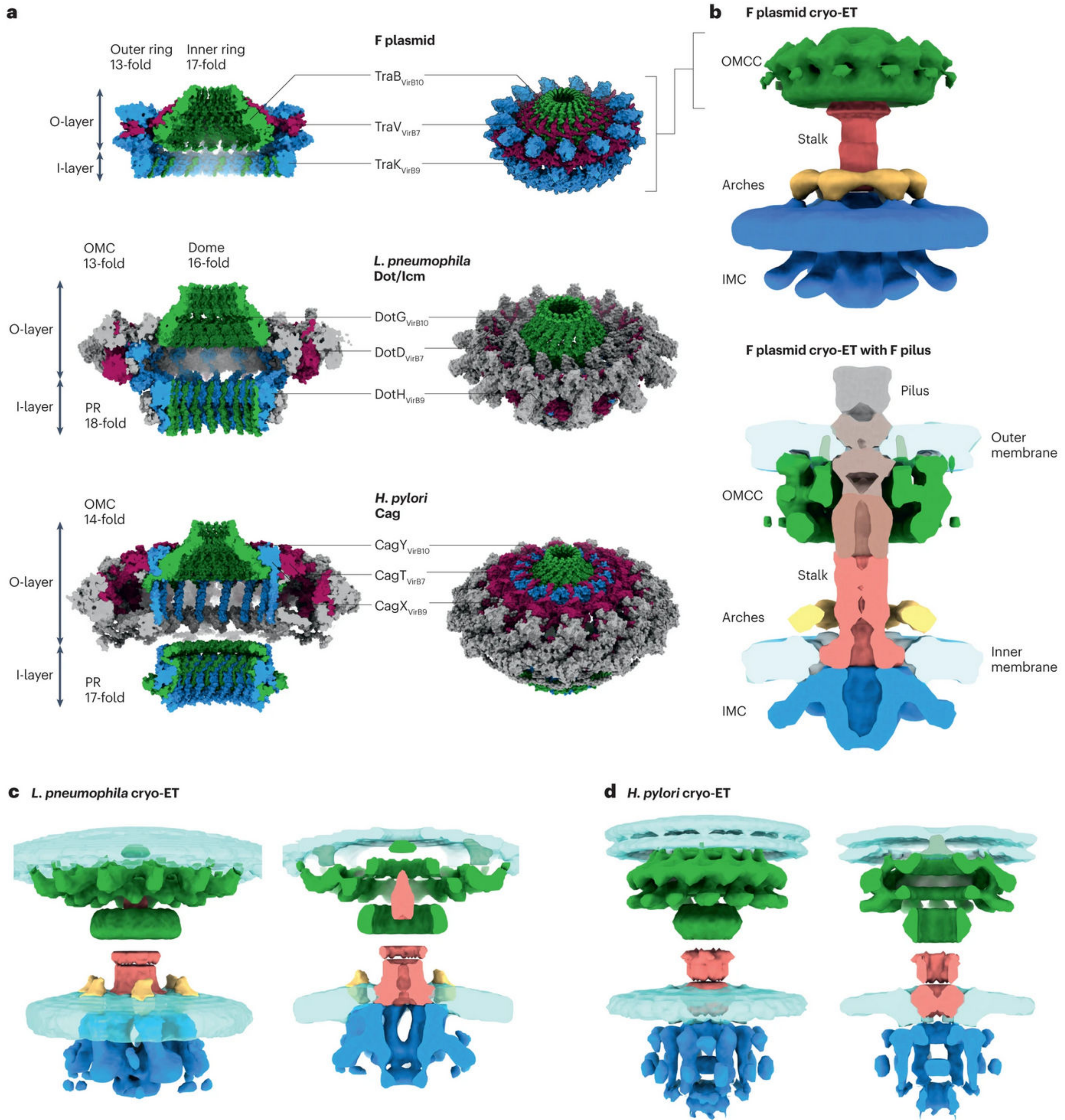


**a**, Global organization to atomic details of the minimized R388-encoded type IV secretion system (T4SS). The entire cryo-electron microscopy (cryo-EM) structure of the R388 T4SS is shown with half-left in cryo-EM density coloured by sub-complexes (Electron Microscopy Data Bank (EMDB) entry 12707, EMD 12708, EMD 12709, EMD 13767 and EMD 12933) and half-right in ribbon and surface semi-transparent representation coloured by proteins (Protein Data Bank (PDB) identifier (ID) 7O3J, PDB ID 7O3T, PDB ID 7O3V, PDB ID 7Q1V and PDB ID 7O1U). In the top-left corner, the cryo-electron tomography (cryo-ET) of pKM101 T4SS density (EMDB 24098 and 24100) coloured by sub-complexes is displayed to show that the structure of purified R388 T4SS is similar to the in situ T4SS structure. For each sub-complex, structure details, symmetry and membrane localization are indicated. Black dashed lines demarcate the boundaries of the outer membrane and inner membrane. **b**, Model of pilus biogenesis mechanism. The T4SS is schematically represented in slice view and coloured by protein. Four states are shown: (1) T4SS in similar state to that observed by cryo-EM and shown in part **a**. (2) The pilus biogenesis state with VirB11 bound at the bottom of VirB4; VirB2 is extracted from the inner membrane and recruited to VirB6 through the coordinated actions of the VirB4–VirB11 ATPases. (3) As layers of VirB2 are recruited, the pilus grows from the VirB6 assembly sites and VirB5 remains at the pilus tip. (4) As the pilus grows, the O-layer of the outer membrane core complex (OMCC) opens up and the pilus with VirB5 at the tip extends into the extracellular milieu to establish contact with potential recipient cells. IMC, inner membrane complex. Part **a** adapted from ref. [14](#), CC BY 4.0

(<https://creativecommons.org/licenses/by/4.0/>).

# Fig. 3: Structural organization of expanded type IV secretion system.

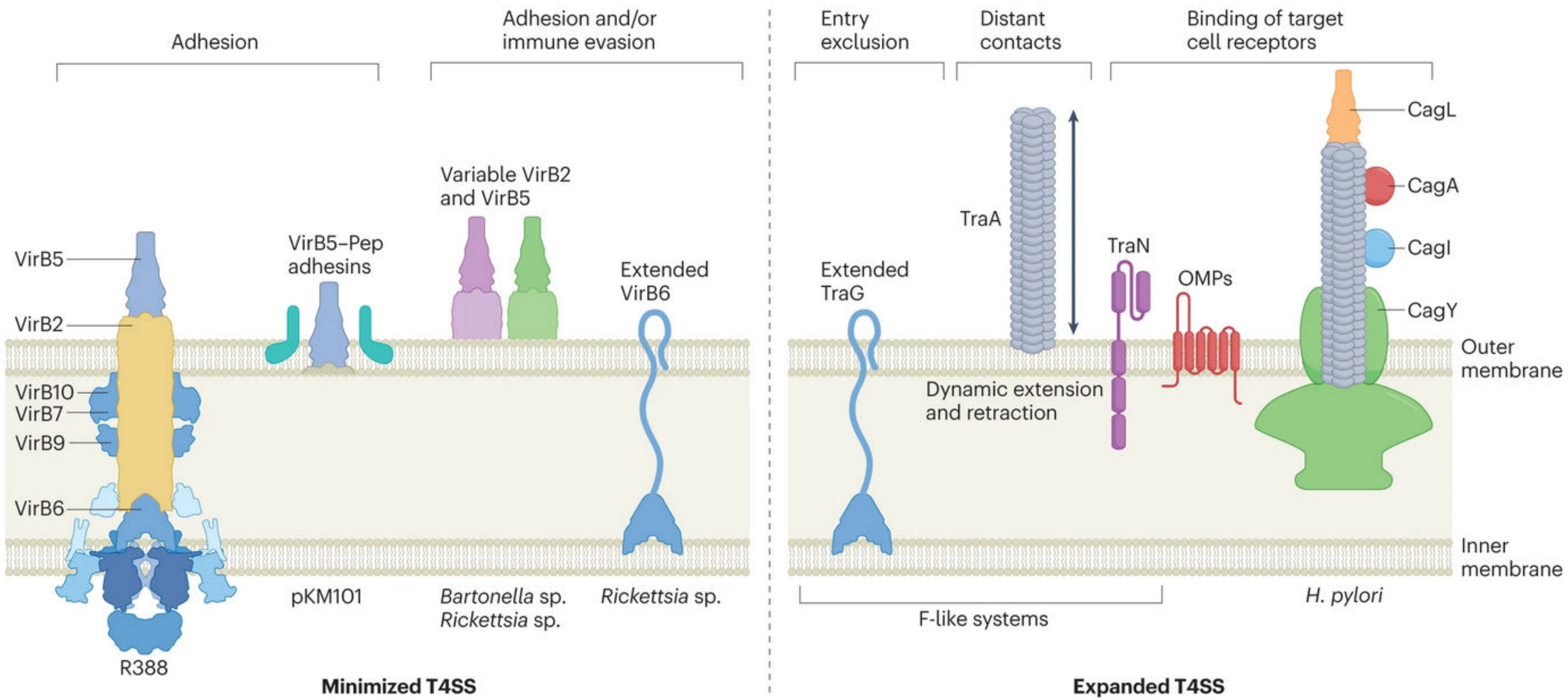
From: [Structural and functional diversity of type IV secretion systems](#)



**a**, Three expanded type IV secretion system (T4SS) outer membrane core complex (OMCC) structures are shown. The OMCCs of the F plasmid (Protein Data Bank (PDB) identifier (ID) 7OKN and PDB ID 7OKO), *Legionella pneumophila* (PDB ID 7MUS) and *Helicobacter pylori* (PDB ID 6X6S and 6X6J) are shown in surface representation and coloured in dark red, blue and green for the VirB7-like, VirB9-like and VirB10-like proteins, respectively, and in grey for other components. Notably, *L. pneumophila* and *H. pylori* OMCCs contain an outer membrane cap (OMC) and a periplasmic ring (PR). **b**, Cryo-electron tomography (cryo-ET) maps of the F plasmid with and without pilus. The maps (Electron Microscopy Data Bank (EMDB) entry 9344 and 9347) are coloured by sub-complexes (that is, green for the OMCC, red for the stalk, yellow for the arches, blue for the inner membrane complex (IMC) and grey for the pilus). The junction of the pilus and stalk is not well defined. **c**, Cryo-ET map of the *L. pneumophila* T4SS (EMDB entry 7611 and 7612) coloured as in part **b**, in front and slice view. **d**, Cryo-ET of the *H. pylori* T4SS (EMDB entry 0634 and 0635) coloured as in part **b**, in front and slice view.

# Fig. 4: Examples of type IV secretion system subunit adaptations for functional diversification.

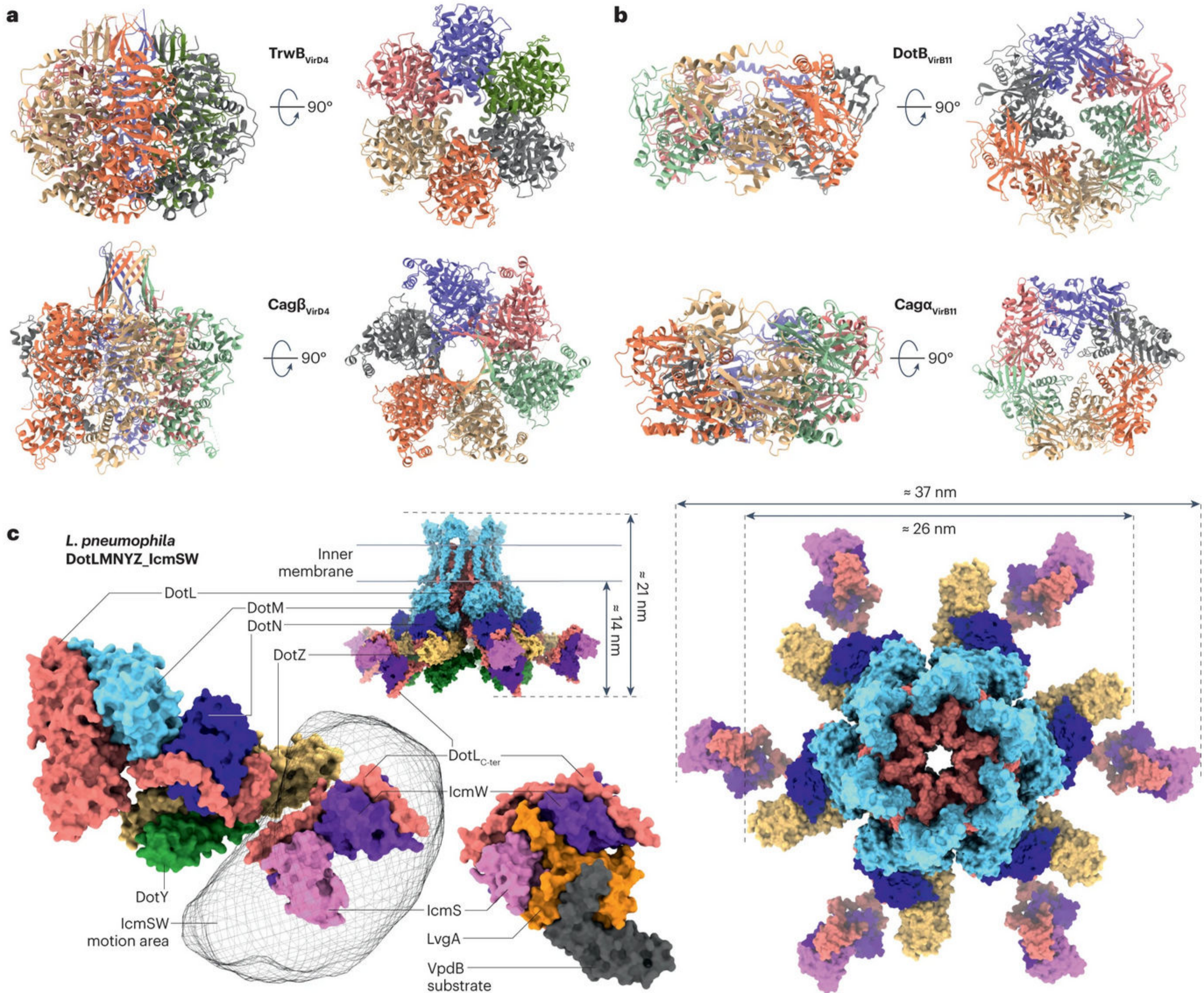
From: [Structural and functional diversity of type IV secretion systems](#)



The R388-encoded type IV secretion system (T4SS) is shown on the left for reference. VirB5 subunits are deployed for binding of target-cell receptors; these subunits can localize at the tips of conjugative pili or on the bacterial cell surface. Some bacteria encode several copies of VirB2 or VirB5 subunits whose variable sequences are postulated to bind different target-cell receptors or contribute to evasion of the host immune system. Extended VirB6 subunits carry large hydrophilic domains, several of which have been shown or are implicated in localizing at the cell surface to promote adhesion or immunomodulation, or blocking redundant plasmid transfer. F systems elaborate F pili that dynamically extend and retract to establish contacts with potential recipient cells at a distance. F systems also code for TraN subunits, whose extracellular domains interact with outer membrane proteins (OMPs) on recipient cells to promote F plasmid transfer and specify plasmid host range. Several T4SSs possess variant forms of the VirB7–VirB9–VirB10 core complex subunits, as exemplified for CagY in the *Helicobacter pylori* Cag system. The *H. pylori* system elaborates a conjugative pilus, which is decorated by other Cag subunits and the CagA secretion substrate. Various T4SSs functionally interact with other surface adhesins, such as pKM101-encoded Pep or *H. pylori* OMPs, to promote target-cell binding.

## Fig. 5: Structure of VirD4-like and VirB11-like ATPases.

From: [Structural and functional diversity of type IV secretion systems](#)

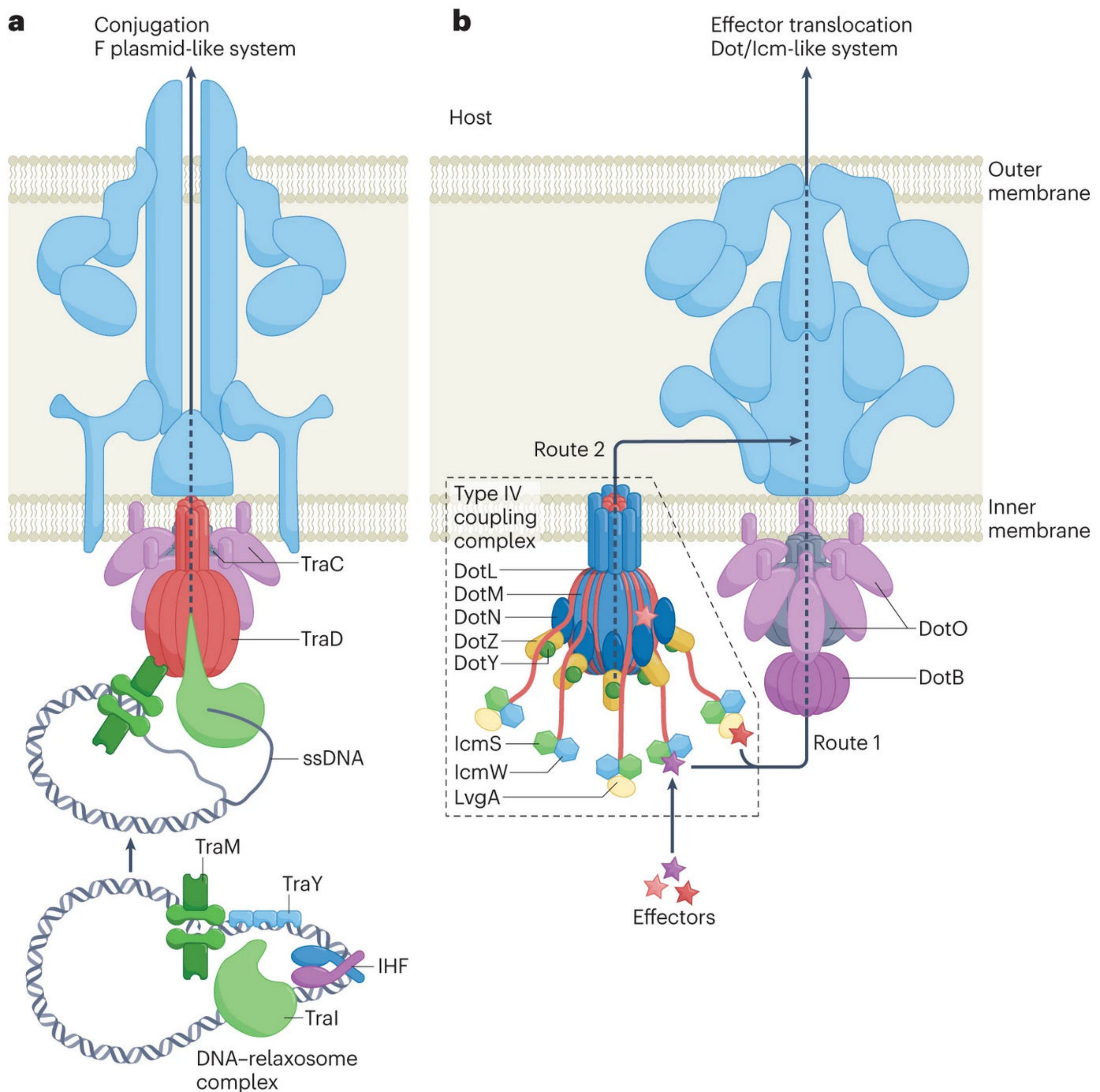


**a**, Side view (left) and top view (right) of two VirD4-like ATPase structures: hexameric TrwB from R388 plasmid (Protein Data Bank (PDB) identifier (ID) 1GKI) and hexameric Cagβ from *Helicobacter pylori* (PDB ID 8DOL). Structures are shown in ribbon representation and coloured by monomer. **b**, Side view (left) and top view (right) of two VirB11-like ATPase structures; hexameric DotB from *Legionella pneumophila* (PDB ID 6GEF) and hexameric Cagα from *H. pylori* (PDB ID 1NLZ). Structures are shown in ribbon representation and coloured by monomer. **c**, Organization and structure of type IV coupling complex (T4CC) from *L. pneumophila*. The monomeric cryo-electron microscopy (cryo-EM) structure of the T4CC (PDB ID 6SZ9) is shown in surface representation and coloured by protein: VirD4-like DotL in red, DotM in cyan, DotN in blue, DotZ in yellow, DotY in green, IcmS in pink and IcmW in purple. The module made up of the extreme C terminus of (DotL<sub>C-ter</sub>) and IcmSW is flexible, and its motion area is represented in mesh. Crystal structure of the DotL<sub>C-ter</sub>-IcmSW module in the presence of LvgA adaptor (orange) and VpdB substrate (black) is shown (PDB ID 7BWK). On the right, a model of the hexameric T4CC structure is shown in top view using the same colour coding as in part **c**.



# Fig. 6: Models for substrate recruitment and transport through the type IV secretion system.

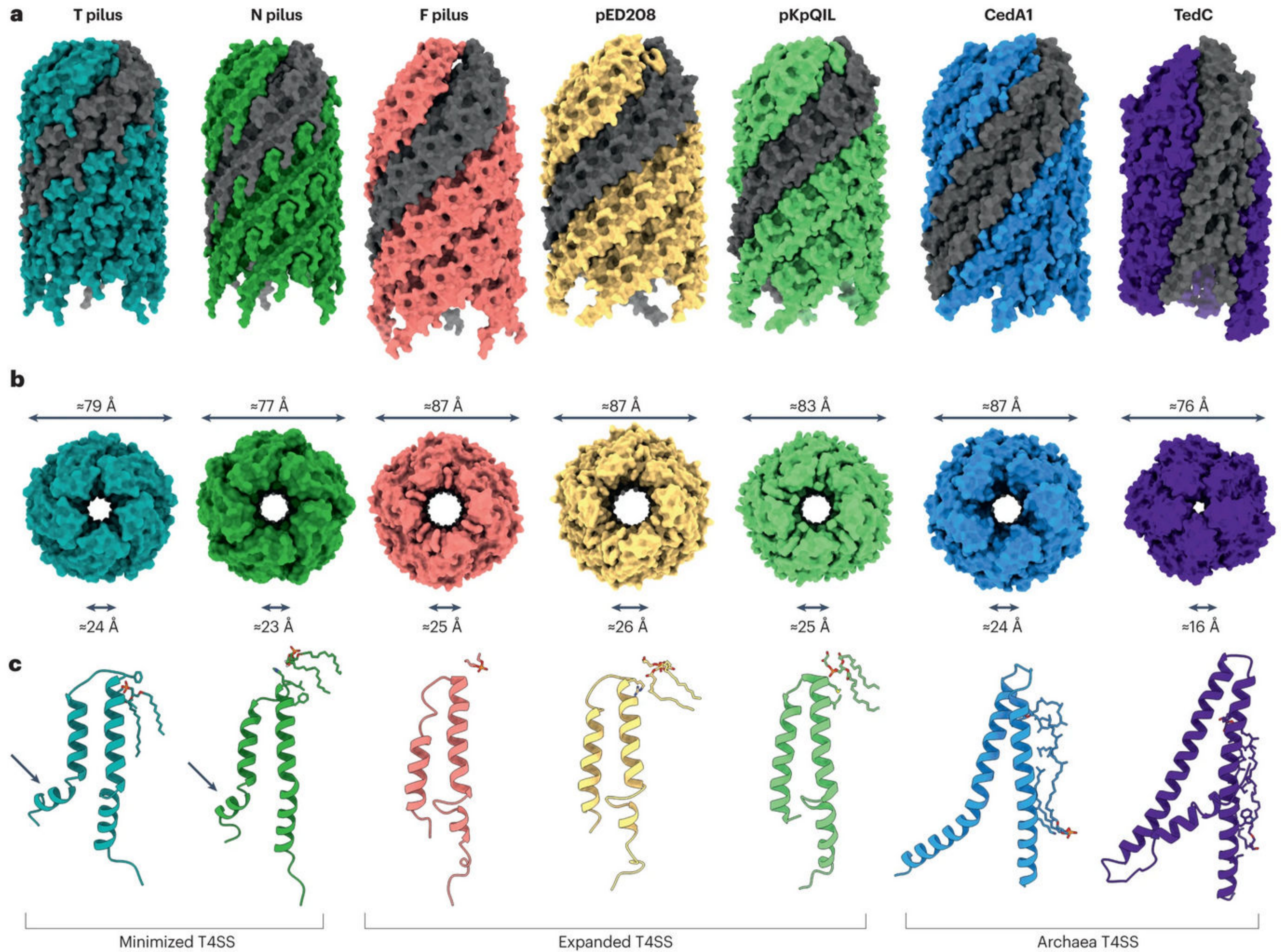
From: [Structural and functional diversity of type IV secretion systems](#)



**a**, Conjugative type IV secretion system (T4SS) recruitment and secretion mechanism model. Silhouette of F plasmid T4SS is shown in blue. First, the DNA is processed by a relaxosomal complex made of TraM (dark green), TraY (turquoise), IHF (purple and dark blue) and Tral (light green). The relaxosome is recruited by TraD<sub>VirD4</sub> ATPase, which energizes the secretion of the Tral–single-stranded DNA (ssDNA) through the T4SS apparatus into the host. The relative position of TraD<sub>VirD4</sub> and the global organization of the inner membrane complex during DNA secretion are unknown. **b**, T4SS effector recruitment and secretion mechanism model. Silhouette of *Legionella pneumophila* Dot/Icm T4SS is shown in blue. The type IV coupling complex (T4CC) acts as an effector recruitment platform and is schematically represented and positioned beside the complex formed by the hexameric dimers of DotO and DotB, although its precise localization is unknown. Effector proteins are captured by the T4CC at different binding sites and DotL<sub>VirD4</sub> energizes substrate translocation via one of two possible routes across the inner membrane. Route 1: the T4CC feeds substrates into the DotO–DotB energy centre at the base of the T4SS channel for transit in one step across the entire cell envelope. Route 2: the T4CC feeds substrates into the lumen of the DotL hexamer for delivery across the inner membrane. In a second translocation step, substrates are recruited from the periplasm by the T4SS channel for passage to the cell surface and into target cells. Part **b** adapted with permission from ref. <sup>28</sup>. Microbiology Society.

# Fig. 7: Structure comparison between minimal, expanded and archaea pilus.

From: [Structural and functional diversity of type IV secretion systems](#)



**a**, Side view of all known pilus structures. Pilus structures (Protein Data Bank (PDB) identifier (ID) 8EXH *Agrobacterium tumefaciens* T pilus, PDB ID 8CW4 *Escherichia coli* N pilus, PDB ID 5LER *E. coli* F pilus, PDB ID 5LEG *Salmonella enterica* subsp. *enterica* serovar Typhimurium pED208, PDB ID 7JSV *Klebsiella pneumoniae* pKpQIL, PDB ID 8DFU *Aeropyrum pernix* CedA1 and PDB ID 8DFT *Pyrobaculum calidifontis* TedC) are in surface representation with one strand coloured in grey. **b**, Top view of pilus structures. Diameter and lumen sizes are indicated. **c**, For each pilus, one monomer of VirB2 with its lipid is shown in ribbon representation. The arrows in the minimized type IV secretion systems (T4SSs) highlight the presence of a 'kink', which is characteristic of this group.

Parts **a** and **b** adapted from ref. [108](#), CC BY 4.0 (<https://creativecommons.org/licenses/by/4.0/>).

966 **Table of content:**

967 In this Review, Costa and colleagues summarise the current knowledge of type IV secretion system (T4SS)  
968 functioning in Gram-negative bacteria, with a focus on their architectures and adaptations for specialised  
969 functions. They also explore the biogenesis pathways and spatial localization of T4SSs.

970

971 **Glossary**

972

973 **Conjugative Pili:**

974 Helical hair-like appendages formed by protein-phospholipid complexes that assemble on the surface of bacteria  
975 and can act as conduits for DNA transfer between donor and recipient bacteria.

976

977 **Biotic and abiotic adhesion:**

978 The attachment of microorganisms to living (biotic) or non-living (abiotic) surfaces, a process that typically  
979 facilitates biofilm formation, niche establishment, or infection.

980

981 **Bacterial conjugation:**

982 Type of horizontal gene transfer in bacteria where genetic material, such as plasmids containing genes for  
983 antibiotic resistance, is transferred from a donor bacterium to a recipient bacterium.

984

985 **Effector:**

986 Bacterial protein, often secreted through a dedicated secretion system, that interacts with and manipulates  
987 cellular processes within a host organism, promoting bacterial survival, colonization, or infection.

988

989 **Cryo-electron microscopy (cryo-EM):**

990 Electron microscopy imaging technique that involves freezing samples in vitreous ice to preserve their native  
991 state and is used to visualize the three-dimensional structure of biological molecules and complexes at near-  
992 atomic resolution.

993

994 **Conjugative plasmid:**

995 A type of a bacterial plasmid that encodes a conjugative machinery, through which the plasmid and its cargoes  
996 of antimicrobial resistance genes, virulence factors, or other fitness traits are delivered between bacterial cells.

997

998 **Polytopic topology:**

999 Protein structure that contains multiple transmembrane segments embedded in the cell membrane.  
1000  
1001 **Co-evolution of proteins:**  
1002 The reciprocal influence and evolution patterns between two proteins that interact or are dependent on each  
1003 other for function, and have evolved in a coordinated, non-random manner reflecting their mutual adaptation  
1004 over time.  
1005  
1006 **Site-directed mutagenesis:**  
1007 Molecular biology technique used to introduce specific nucleotide mutations into DNA sequences, with the  
1008 purpose of studying their effects on protein structure and function.  
1009  
1010 **Cryo-electron tomography (cryo-ET):**  
1011 Specialized variation of cryo-EM that enables the visualization of large cellular components or organelles within  
1012 their cellular environment.  
1013  
1014 **Cryo-focused ion beam (cryo-FIB):**  
1015 A technique used to prepare samples for cryo-electron microscopy by thinning frozen samples with a focused  
1016 ion beam, leading to an improved signal-to-noise ratio and resolution in the imaging of biological samples.  
1017  
1018 **Toll-like receptor:**  
1019 A family of pattern recognition receptors (PRR) in the immune system that specifically recognize conserved  
1020 patterns in pathogens and triggers an immune response.  
1021  
1022 **Crosslinking:**  
1023 Artificial formation of covalent bonds by a crosslinker between different molecules that interact or co-localize  
1024 within a biological sample, with the common application of studying protein-protein or protein-ligand  
1025 interactions.  
1026  
1027 **Rotational raise:**  
1028 Angle at which adjacent rings stack in helical assemblies, influencing the overall helical symmetry and packing  
1029 of the structure.  
1030  
1031 **Translocation signal:**  
1032 Specific amino acid sequence that confers recognition of a protein as a substrate for a dedicated transport  
1033 machinery for delivery to a specific cellular location, the extracellular milieu, or another bacterial or eukaryotic  
1034 cell.  
1035  
1036 **Correlative light and electron microscopy (CLEM):**

1037 Imaging technique that combines fluorescence microscopy and electron microscopy to correlate high-resolution  
1038 structural information with specific molecular or cellular labelling in the same sample.

1039

1040 **Nanobodies:**

1041 Single-domain antibody fragments derived from heavy-chain-only IgG antibodies that are naturally found in the  
1042 Camelidae family, which includes camels, llamas, and alpacas.

1043

1044 **Adhesins:**

1045 Proteins found on the surface of cells that facilitate attachment to other biotic or abiotic surfaces.

1046

1047 **Biofilm:**

1048 An assemblage of bacteria on a biotic or abiotic surface, often with a defined architecture, that is embedded in  
1049 an extracellular matrix typically composed of proteins, DNA, lipids and other biological molecules.

1050

1051 **Relaxosome:**

1052 A complex of proteins responsible for specific nicking of the double-stranded DNA, unwinding of DNA strands  
1053 and delivering the single-stranded DNA transfer intermediate to the type IV secretion apparatus prior to  
1054 conjugation.

1055